FEEDBACK ERROR LEARNING AT THE MUSCLE LEVEL: A UNIFIED MODEL OF HUMAN MOTOR ADAPTATION TO STABLE AND UNSTABLE DYNAMICS

TEE KENG PENG

(B.Eng.(Hons.),NUS)

A THESIS SUBMITTED

FOR THE DEGREE OF MASTER OF ENGINEERING

DEPARTMENT OF MECHANICAL ENGINEERING

NATIONAL UNIVERSITY OF SINGAPORE

2003

Acknowledgements

First of all, I wish to express sincere thanks to main supervisor Dr Etienne Burdet for introducing me to the fascinating field of human motor adaptation, for spending time and energy to guide me in research, and for giving me the opportunity to collaborate with the Advanced Telecommunications Research Institute International (ATR) in Japan, an experience which I found immensely rewarding.

I am also thankful to co-supervisor Dr Chew Chee Meng, who has closely followed my progress in the last two and a half years, continually offering fresh perspectives and helping to hone my critical thinking skills.

Special thanks to Ganesh Gowrishankar, for being a sincere friend and a great help to my project. The initial study of muscle level feedback error learning on single joint movements was done together with him.

At ATR, fruitful discussions with Dave Franklin, Ted Milner, Mitsuo Kawato and Rieko Osu elucidated concepts and experimental support crucial to the implementation of a physiologically plausible learning model. I am thankful to ATR for sponsoring my flight and accommodation during my month-long stay in Japan.

To the laboratory officers Ms Tshin Oi Meng, Mrs Ooi-Toh Chew Hoey, Mrs Hamidah Bte Jasman, Mr Zhang Yao Ming and Mr Yee Choon Seng, thanks very much for your dedicated, timely and efficient handling of administrative and technical matters.

Last but not least, I am grateful to my parents, siblings and Ying Ying for believing in me and being with me every step of the way.

Table of Contents

List of Figures

List of Tables

Summary

Humans have striking capabilities to perform many complex motor tasks such as carving and manipulating objects. This means that humans can learn to compensate skillfully for the forces arising from the interaction with the environment. As an attempt to understand motor adaptation, this thesis introduces a model of neural adaptation to novel dynamics and simulates its behavior in representative stable and unstable environments.

Psychophysical experiments have shown that humans are able to adapt to stable dynamics in order to perform tasks successfully (Shadmehr and Mussa-Ivaldi 1994, Conditt and Mussa-Ivaldi 1997, Shadmehr and Holcomb 1996). Recent experiments (Burdet *et al* 2001A) further show that humans are also able to adapt to unstable dynamics, and suggest that the central nervous system (CNS) can control endpoint impedance to counteract instability with low metabolic cost. However, previous models of motor adaptation cannot stabilize unstable dynamics, and learn stable dynamics with transients different from that found in experiments.

Our proposed controller assumes that the adaptation mechanism, realized in muscle space, comprises three elements:

- In each muscle, the stretch reflex, representative of the novel dynamics, is utilized to update the feedforward command. This is similar to feedback error learning (Albus 1975, Kawato *et al* 1987), but is realized here in muscle rather than joint space.
- A stretched muscle induces correlated reflex both in this muscle and in the antagonist, i.e. cross reflex.

- Selective deactivation decreases the coactivation of agonist-antagonist muscles not required to stabilize movement.

Simulations on a 2-link 6-muscle model demonstrate the capabilities of the proposed algorithm. Feedforward motor commands, which produce inverse dynamics (IDM) compensating for reproducible dynamics and anisotropic impedance counteracting irreproducible effects, are gradually learned in repeated trials. The simulated motion trajectories, evolution of muscle activity, and final endpoint impedance are consistent with experimental results (Burdet *et al* 2001A, Franklin *et al* 2003A, Osu *et al* 2003, Franklin *et al* 2003B). Furthermore, this novel nonlinear adaptive controller is the first that is able to learn appropriate motor commands compensating for both stable and unstable dynamics.

Sensitivity analysis shows that learning is robust to large variations of parameters. Neither learning nor motion control is impeded by an increase of noise of up to 1.5 times, by a large delay in reflex of up to 200ms, and by the full range of cross reflex magnitudes from 0 to 1. In unstable dynamics, feedback error learning in muscles results in consecutive motions alternating on either side of the mean trajectory. This increases coactivation of agonist-antagonist muscles, hence providing larger arm impedance that counteracts the instability. As a consequence, cross reflexes, although identified in EMG (Franklin *et al* 2003B), are not indispensable to learning stable movements in unstable dynamics. While the transients and asymptotic impedance depend on the learning parameters, the qualitative evolution features predicted by the model are generally similar to the behavior observed in psychophysical experiments.

Simulations are also performed to predict the adaptation to representative dynamic environments, which future psychophysical experiments may validate. Examining the adaptation to instabilities in various directions, we find that while impedance generally increases in the direction of instability, it tends to converge along the stiffness axis of the maximally stretched muscle pair. In addition, impedance increases monotonously with the magnitude of instability to provide about the same trajectory deviation in various dynamic environments. Finally, the modeled controller is able to learn and coordinate motor commands in environments requiring modification of both force and impedance.

Such computational models, using only measurable variables and simple computation, may be used to simulate the effect of neuro-muscular disorders on movement control, to develop better controllers for neural prostheses and to design novel rehabilitation approaches. While developing this novel model, the author has also contributed related works including the realization of a hybrid IDM/impedance learning controller to stabilize unstable dynamics (Tee 2001, Burdet *et al* 2001C), a model of endpoint force and impedance (Tee *et al* 2003A, Tee *et al* 2003B) and a study of stability (Burdet *et al* 2001B) in human movements.

1 Introduction

1.1 Motivation and Goal

A common conception holds that humans can be distinguished from animals by their use of tools (Whiten *et al* 1998). Despite evidence that tool manipulation is not exclusive to humans (de Waal 1999,Weir *et al* 2002), the ability of humans to learn to wield a wide range of tools dexterously in different environments is exceptional. How are humans able to constantly adapt to novel tasks with distinct dynamics? As a specific example, let us consider the novel task of sculpting, which requires learning to produce the forces to move the chisel on the material surface and at the same time compensating for any potential destabilization due to material excrescencies and motor noise. To accomplish complex tasks such as sculpting, the central nervous system (CNS) coordinates muscles in the limbs to produce the appropriate force and impedance (i.e. the resistance to infinitesimal perturbations applied at the hand) during movement.

When an action is performed for the first time, there is generally a need to monitor the movement continuously. However, when the action is repeated, the motion gradually becomes automatic, requiring less and less feedback control. In a similar way, a very successful algorithm, *feedback error learning* (FEL) (Albus 1975, Kawato *et al* 1987), learns the feedforward force to perform stable actions by minimizing feedback during repeated trials. Several studies suggest that the oculo-motor system uses a similar strategy (Yamamoto *et al* 2001, Kawato 1999, Gomi *et al* 1998, Kobayashi *et al* 1998, Shidara *et al* 1993). In multi-joint arm movements, FEL was found to be consistent with patterns of adaptation to stable dynamics (Shadmehr and Mussa-Ivaldi 1994, Conditt and Mussa-Ivaldi 1997, Shadmehr and Holcomb 1997, Krakauer *et al* 1999). However, conventional

FEL cannot explain (Burdet *et al* 2001B, Osu *et al* 2003) the adaptation to unstable dynamics that are recently investigated (Milner and Cloutier 1993, Burdet *et al* 2001A).

A novel algorithm is needed to explain how the CNS learns to perform motion in both stable and unstable dynamics. To address this need, we have developed a computational model that will be described in this thesis. The model suggests how the CNS adapts muscle forces in order to successfully perform novel motor tasks. It assumes that sensor afferents relay feedback to the CNS, which uses it to modulate feedforward command, and considers motor output variability. This model uses measurable variables and parameters such as muscle activation, hand force and trajectory, and is therefore testable. Despite being based on only a few assumptions, it is able to predict the main learning features observed in (Franklin *et al* 2003A, Osu *et al* 2003, Franklin *et al* 2003B, Franklin *et al* 2002).

1.2 Related Experimental Results

In recent experiments (Burdet *et al* 2001A, Franklin *et al* 2003A, Osu *et al* 2003, Franklin *et al* 2003B, Franklin *et al* 2002), human subjects performed horizontal reaching arm movements away from the body while interacting with a haptic interface that exerted forces on the hand (Fig. 1). In the null field (NF), the subjects performed straight movements towards the target. Introduction of a novel force field perturbed the movement significantly. However, with practice, all subjects were able to adapt to the force field and perform successful movements. Burdet *et al* 2001A, Franklin *et al* 2003A, Osu *et al* 2003, Franklin *et al* 2003B analysed, in particular, the adaptation to a velocity-dependent force

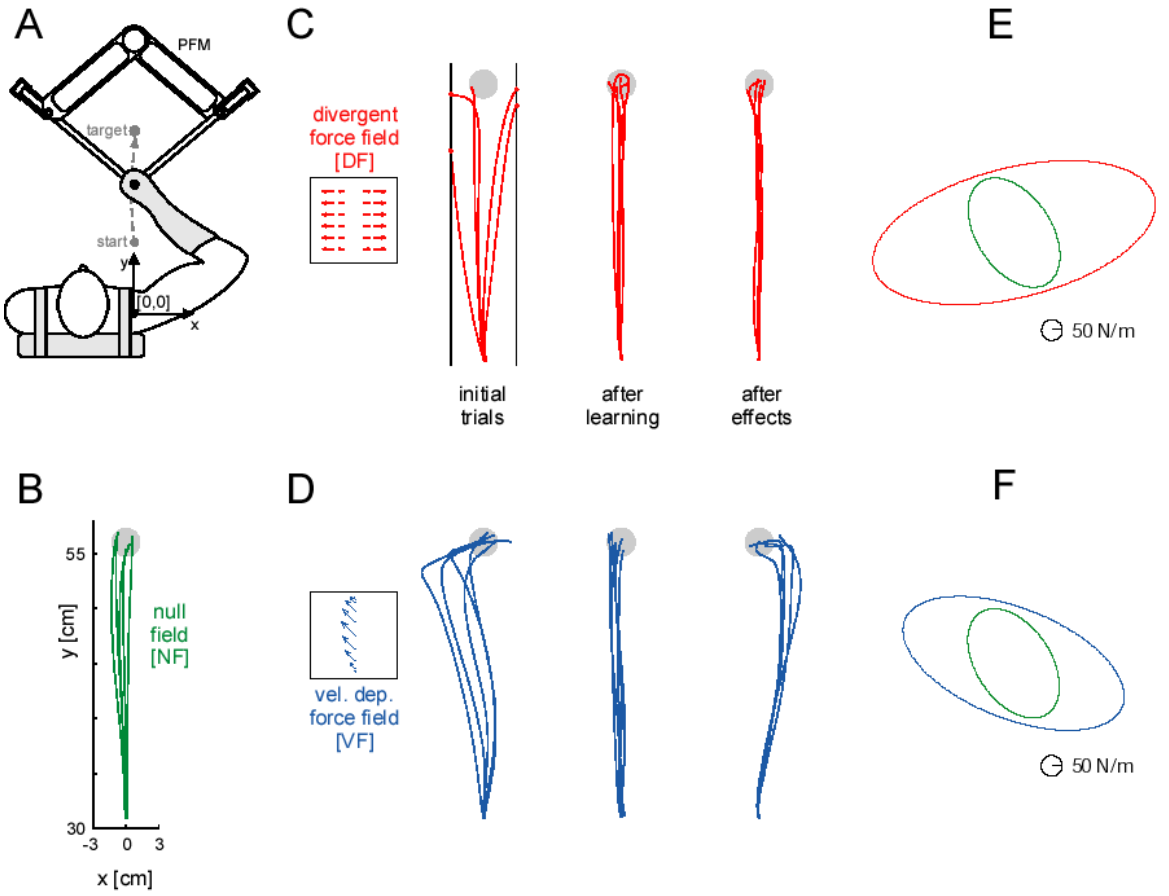

Fig. 1 Motor adaptation experiment of (Burdet *et al* 2001A, Franklin *et al* 2003A, Franklin *et al* 2003B, Osu *et al* 2003). *A*: The subjects adapted to forces produced during movement by a robotic interface. B: Hand trajectories in the null field condition (NF) are almost straight to the target. *C*, *D*: The two kinds of force fields studied and corresponding trajectory adaptation. *E*, *F*: Endpoint stiffness after adaptation to the force fields.

field (VF) producing a stable interaction with the arm, and a divergent force field (DF) producing an unstable interaction. The hand trajectory, endpoint force and stiffness, as well as the electromyogram (EMG) of shoulder, elbow and biarticular muscles were measured during movement, with the following observations:

- When learning VF, the trajectories become similar to NF trajectories in less than 10 trials. In DF, adaptation is slower, with the trajectories becoming similar to NF trajectories after 25 trials.

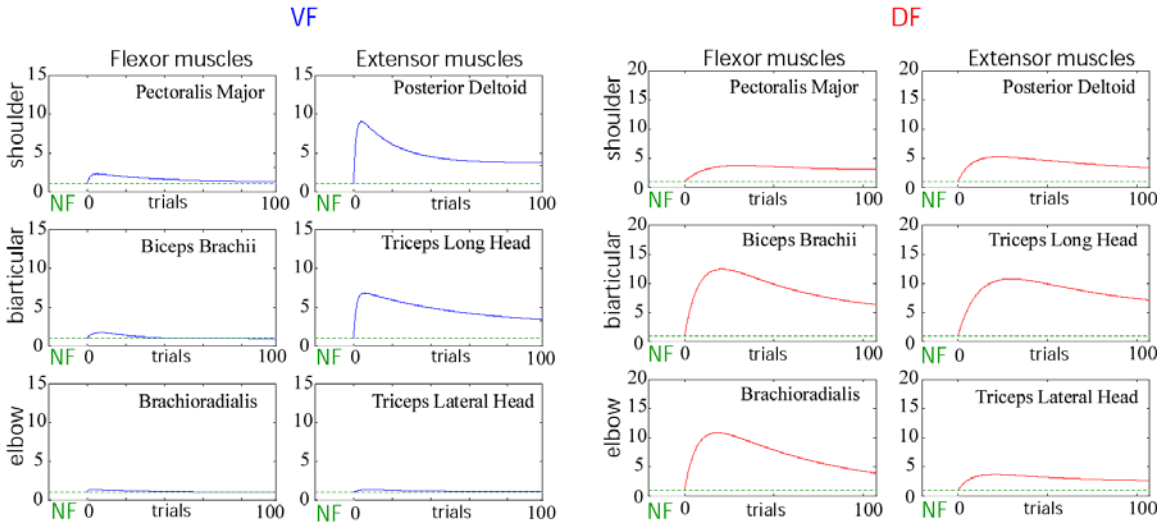

Fig. 2 EMG measurements (Franklin *et al* 2003B) of 6 muscles in the human arm during adaptation to the velocity-dependent force field (VF) and the divergent force field (DF), normalized with respect to EMG in null field (NF). The curves are double exponential functions best-fit with least square error. The 6 muscles form flexor-extensor pairs for the reaching movements studied.

- In both VF and DF, the initial sharp increase of muscle activity due to cocontraction of agonist-antagonist muscles is followed by a gradual relaxation (Fig. 2).
- For VF, when the force field is unexpectedly shut down after adaptation, movements (termed *after effects*) are curved in the direction opposite to the force, suggesting that an inverse dynamics model was acquired during adaptation. The activity of extensor muscles is high after learning.
- During adaptation DF, hand stiffness is increased selectively along the direction of instability (Fig. 1), producing a stability margin (i.e. difference between adapted and environmental stiffness) that is similar to NF stiffness. Correspondingly, after effect trials in DF are characterized by a decrease of deviation relative to NF movements.

- The direction of trajectory error in DF alternates left and right of the mean trajectory during the early stage of learning. This contrasts sharply with trajectory error in VF, which is initially biased to the left and decays in a manner that is consistent with feedback error learning. Both suggest that some feedback error learning is taking place in motor adaptation.
- The initial trials in novel dynamics show an increase of muscle activation that is correlated with muscle stretch. When an agonist muscle is stretched, the antagonist activation will be increased even though the antagonist is not stretched.

1.3 Overview of model

Our novel model describes how muscle activation is adapted to perform successful movements in novel dynamics. It is defined by the three properties:

1. A stretch in a muscle elicits a correlated reflex signal in itself as well as in its antagonist.
2. For each muscle, the reflex feedback is used to update the feedforward command on the next trial, inducing an increase of endpoint impedance.
3. The feedforward cocontraction signals of all muscle pairs decay slowly, and the muscle pair with the largest cocontraction decays faster.

Adaptive compensation for the mean external force is realized through the second property, which is feedback error learning at the muscle level. Although the agonist-antagonist muscle pairs are independent, dynamic coupling arises through feedback error learning with repetition of the movement. This is similar to conventional FEL proposed in

(Kawato *et al* 1987). The first and third properties ensure that the stiffness ellipse is elongated in the direction of instability.

In unstable dynamics consecutive movements deviate in different directions. With the first two properties, it leads to the coactivation of all muscles (Fig. 5). Hence, our algorithm is able to stabilise unstable dynamics, in contrast to FEL (Burdet *et al* 2001B, Burdet *et al* 2003) and also all existing controllers.

In principle, increasing coactivation leads to a more robust control and less trajectory deviation. However, noise is increasing with coactivation. The adaptive controller tends to seek a balance between low deviation and low coactivation.

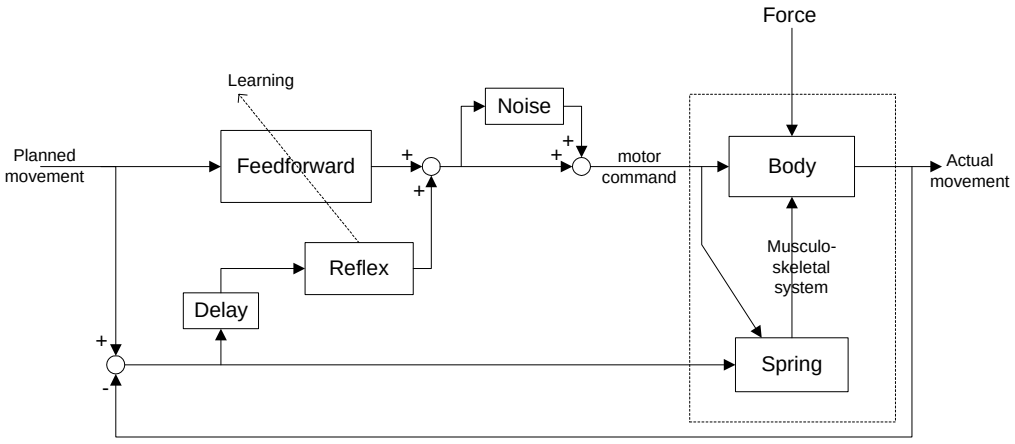

Fig. 3 Dynamics of motion generation, consisting of feedforward, reflex and noise in the motor command, spring-like forces in the muscles, and forces from the environment acting on the moving body part. Error between the actual and planned movements produces a restoring force arising from muscle elasticity and the (delayed) reflexes. Afferent signals that evoke reflexes modulate the descending feedforward from the CNS via feedback error learning.

2 Model of Human Motor Adaptation

Models of human motor adaptation can be broadly classified into two categories: those assuming the Internal Model hypothesis and those assuming the Equilibrium Point Trajectory hypothesis. The Internal Model hypothesis asserts that the CNS acquires internal representations of the dynamics of interactions with the external world, which it uses to predict motor commands and execute movements successfully. The Equilibrium Point Trajectory hypothesis postulates that, to learn motor skills, the CNS only needs to utilize kinematic information in the form of an equilibrium trajectory. This is possible due to muscle viscoelasticity and reflexes, which generate servo action whenever there is an error between the actual state and the equilibrium state.

Our model of motor adaptation is in line with the Internal Model hypothesis, and postulates that stretch reflexes, elicited by trajectory error, contribute to the formation of an inverse dynamics model and to an increase of muscle coactivation.

Previous models have focused on the learning of inverse dynamics in stable interactions using neural network (Kawato *et al* 1987) or adaptive control (Burdet 1996). Stroeve 1999 modelled a motor control system that used a single neural network to learn both the inverse dynamics model and impedance in a stable interaction. However, it is unclear if these models will be successful in predicting the necessary increase of impedance in unstable interactions. By considering the learning process at the muscle level, our model provides a novel unified framework for learning both the inverse dynamics model and the necessary impedance for stability, in both stable and unstable interactions.

In the following sections, we shall examine how the main dynamic components in movement control are modeled. These are namely the arm dynamics, muscle viscoelasticity and reflexes, motor noise and the feedforward motor command. Finally we shall look at how our algorithm leads to the learning of appropriate feedforward motor command in both stable and unstable dynamics.

2.1 Movement control

The dynamics of motion generation are shown in Fig. 3. A list of all the equations governing the model is given in Appendix C.

Muscles produce the force to generate movement, as expressed by the following equation:

TASK DYNAMICS = MUSCLE (1)

The task dynamics comprises the dynamics to move the limb, which we model by the rigid-BODY dynamics, and to counteract the external FORCE from the environment:

TASK DYNAMICS = BODY + FORCE (2)

The muscle force stems from the total motor COMMAND comprising the descending (efferent) command and reflexes, and from SPRING, the mechanical impedance (i.e. resistance to infinitesimal perturbation of the state) produced by muscle mechanics:

MUSCLE = COMMAND + SPRING (3)

The motor command can be evaluated from the EMG signal, and impedance from measurements of the restoring force due to small perturbations (Mussa-Ivaldi *et al* 1985,

Burdet *et al* 2000). We further consider that impedance increases with motor command (Hunter and Kearney 1982, Gomi and Osu 1998).

We assume that the motor command is composed of a descending feedforward command (FF), updated with repeated movements; neural feedback, represented by the stretch REFLEX; and motor NOISE that increases with muscle activation:

COMMAND = FF + REFLEX + NOISE (4)

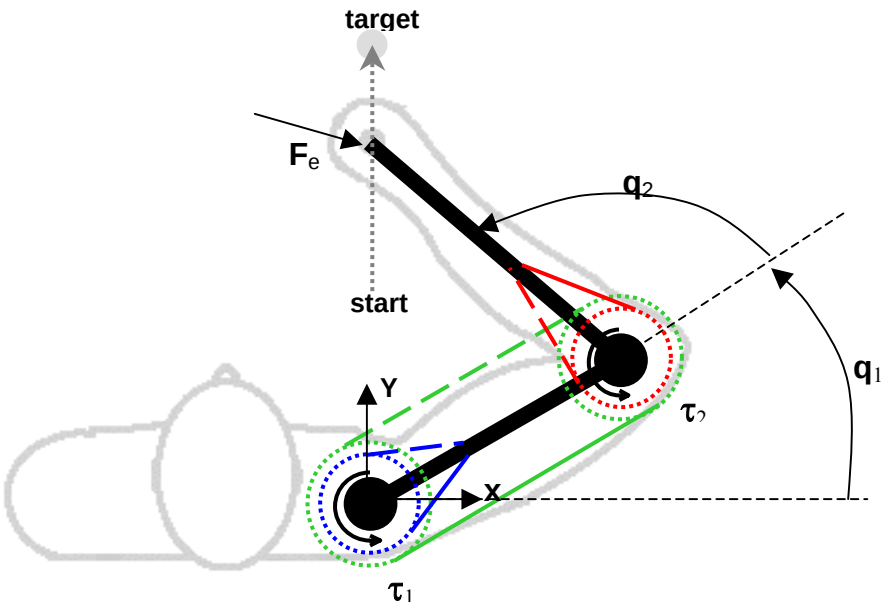

Fig. 4 The arm model used in simulation consists of two segments, two joints and six muscles. *Blue*: shoulder muscles with moment arms ρ_1=ρ_2. *Red*: elbow muscles with moment arms ρ_3=ρ_4. *Green*: biarticular muscles with moment arms ρ_5=ρ_6 at the shoulder and ρ_7=ρ_8 at the elbow. Dashed lines represent flexor muscles while solid lines represent extensor muscles. Hand coordinates (x,y) are relative to the shoulder. τ_1 and τ_2 are the shoulder and elbow torques respectively; q_1 and q_2 are the shoulder and elbow angles respectively. Reaching movement is generated from start to target while interacting with the external force F_e.

Equations (1) to (4) yield

BODY + FORCE = FF + SPRING + REFLEX + NOISE (5)

which describes the dynamics of the arm controlled by the CNS to perform a task. To compute the resulting motion, this equation will be integrated in joint space.

2.2 Rigid Body Kinematics and Dynamics

The kinematic and dynamics transformations between the hand, joint and muscle spaces are summarized in Table 1. Vectors and matrices are denoted in **bold** and scalars in *italic*. In hand space, $\mathbf{x}$ is the hand position, and $\mathbf{F}$ the force exerted on the hand. In joint space, $\mathbf{q}$ is the joint position, $\mathbf{q}_v$ the joint velocity, and $\boldsymbol{\tau}$ the joint torque. In muscle space, $\boldsymbol{\lambda}$ is the vector of muscles lengths, $\boldsymbol{\lambda}_v$ the corresponding velocity and $\mathbf{m}$ the muscle tensions.

Table 1 Kinematic and dynamic transformations between the hand, joint and muscle spaces

hand		joint		muscle	
$\mathbf{x}$	$\longleftarrow$	$\mathbf{q}$	$\longrightarrow$	$\boldsymbol{\lambda}$	position
$\mathbf{v}$	$\xleftarrow{\mathbf{J}\,\mathbf{q}_v}$	$\mathbf{q}_v$	$\xrightarrow{\mathbf{J}_m\,\mathbf{q}_v}$	$\boldsymbol{\lambda}_v$	velocity
$\mathbf{F}$	$\xrightarrow{\mathbf{J}^T\mathbf{F}}$	$\boldsymbol{\tau}$	$\xleftarrow{\mathbf{J}_m{}^T\mathbf{m}}$	$\mathbf{m}$	force
$\mathbf{K}_x$	$\xrightarrow{\mathbf{J}^T\mathbf{K}_x\mathbf{J} + (d\mathbf{J}^T/d\mathbf{q})\mathbf{F}}$	$\mathbf{K}_q$	$\xleftarrow{\mathbf{J}_m{}^T\boldsymbol{\kappa}\mathbf{J}_m}$	$\boldsymbol{\kappa}$	stiffness

The rigid body dynamics have the general form (deWit *et al* 1996):

$$\mathrm{BODY}(\mathbf{q},\mathbf{q}_v,\mathbf{q}_a) = \mathbf{H}(\mathbf{q})\mathbf{q}_a + \mathbf{C}(\mathbf{q},\mathbf{q}_v)\mathbf{q}_v + \mathbf{G}(\mathbf{q}) \qquad (6)$$

where $\mathbf{H}(\mathbf{q})$ denotes the mass matrix, $\mathbf{q}_a$ denotes the joint acceleration, $\mathbf{C}(\mathbf{q},\mathbf{q}_v)\mathbf{q}_v$ denotes Corioli's and centrifugal forces and $\mathbf{G}(\mathbf{q})$ denotes the forces due to gravity. For horizontal movements $\mathbf{G}(\mathbf{q})$ can be neglected.

For the 2-link 6-muscle model which is used in the simulations (Fig. 4), $\mathbf{x}$, $\mathbf{q}$, $\boldsymbol{\tau}$, $\mathbf{F}$ are 2x1 vectors, $\boldsymbol{\lambda}$, $\mathbf{m}$ are 6x1 vectors, $\mathbf{J}_m$ is a 2x6 matrix, $\mathbf{J}$, $\mathbf{K}_x$, $\mathbf{K}_q$ are 2x2 matrices and $\mathbf{K}_m$ is a 6x6 matrix. The indices are labeled as follows:

- In hand space, $\mathbf{x}=[x_1\ x_2]^T$: 1 for x-position, and 2 for y-position relative to shoulder joint.
- In joint space, $\mathbf{q}=[q_1\ q_2]^T$: 1 for shoulder, and 2 for elbow.
- In muscle space, $\mathbf{m}=[m_1\ m_2\ \ldots m_6]^T$: 1 and 2 for shoulder monoarticular muscles, 3 and 4 for elbow monoarticular muscles, 5 and 6 for biarticular muscles.

The transformation matrix between joint space and muscle space corresponds to the moment arms ρ_1 to ρ_8 of the six muscles at the two joints, and we assume them to be constant:

$$\mathbf{J}_{\mathrm{m}} = \begin{bmatrix} \rho_1 & -\rho_2 & 0 & 0 & \rho_5 & -\rho_6 \\ 0 & 0 & \rho_3 & -\rho_4 & \rho_7 & \rho_8 \end{bmatrix}^{\mathrm{T}} \tag{7}$$

All the above transformations, as well as the rigid body dynamics model, are described in Appendices A and B respectively.

2.3 Muscle viscoelasticity and reflexes

The muscle spring-like property, i.e. the phenomenon where the hand returns to the undisturbed trajectory after a perturbation (Milner 1993, Won and Hogan 1995), stems from muscle viscoelasticity and from stretch reflex. Their main characteristics are as follows:

- When there is a displacement in muscle length, there is an immediate increase in muscle force arising from muscle elasticity, which is due to the mechanical properties of cross-bridges and passive tissue.
- This response is supplemented by the delayed stretch reflex mediated through afferent pathways.

- Both muscle stiffness and reflex gain increase with muscle force (Sinkjaer 1988).
- Reflex EMG has been found to have a linear relation with muscle stretch velocity (Eng and Hoffer 1997, Nakazawa 2001).
- Reflex activity of antagonist increases even though only agonist muscle is stretched (Milner 1995, Franklin 2003B).

Both muscle viscoelasticity and reflex are modeled in muscle space as some proportional-and-derivative terms of muscle stretch $\Delta\lambda(t)$. For each muscle, the viscoelastic restoring force is represented as:

$$s(t)= \kappa\,[\Delta\lambda(t) + \kappa_d\,\Delta\lambda_v(t)]\,I_{\{\Delta\lambda(t)>0\}} \quad (8)$$

where κ is the muscle stiffness, κ_d is the ratio of muscle viscosity to stiffness, I is the Kronecker indicator function defined by $I_{condition}\equiv 1$ when the *condition* is fulfilled and 0 otherwise. The stretch $\Delta\lambda = \lambda-\lambda_d$ is computed relative to the planned trajectory in muscle coordinates, $\lambda_d(t)$.

The reflexes r_a and r_{aa} in agonist-antagonist muscle pair are modeled as

$$r_a\,(t)= e_a(t) + \beta\, e_{aa}(t) \quad (9)$$

$$r_{aa}(t) = e_{aa}(t) + \beta\, e_a(t)$$

where

$$e(t)= g\,[\Delta\lambda(t-\phi) + g_d\,\Delta\lambda_v(t-\phi)]\,I_{\{\Delta\lambda(t)>0\}} \quad (10)$$

is the error signal of each muscle, β yields the strength of cross reflexes and ϕ is the reflex delay. The subscripts $_a$ and $_{aa}$ denote agonist and antagonist muscles respectively.

The results of (Hunter and Kearney 1982, Gomi and Osu 1998) show that impedance increases with the force produced. Similarly, we assume that both the intrinsic stiffness κ and the reflex gain g increase linearly with muscle activity. For each muscle,

$$\kappa(t) = \kappa_0 + \kappa_1 m(t) \quad \text{and} \quad g(t) = g_0 + g_1 m(t) . \tag{11}$$

κ_0, κ_1, g_0 and g_1 are chosen to be identical across all muscles. With this constraint, each muscle has an equal likelihood of increasing its stiffness and reflex gain based on the amount of stretch it is subjected to. The muscles that are more activated and/or stretched will have correspondingly higher stiffness and reflex gains.

2.4 Motor Noise

During planning and execution of movements by the CNS, noise at the neural level corrupts the signals that encode sensory information and motor command. This is manifested in higher cognitive levels as variability in visual and proprioceptive perception (Foley and Held 1972, van Beers *et al* 1998), motor output (Fitts 1954, Schmidt *et al* 1979), and internal estimation of the body's state by the CNS (Festinger and Canon 1965, Wolpert *et al* 1995). For simplicity, we model only the overall effect of these noise sources as deviation in muscle tension.

Empirical findings, in isometric force production (Schmidt *et al* 1979, Meyer *et al* 1998, Jones *et al* 2002) and in movement (Nakano *et al* 2002), show that the standard deviation of force produced in the muscles scales linearly with the mean force. These evidences directly support the long-held assumption that motor noise is signal dependent. Hence we require motor noise to be monotonously increasing with the total motor

command comprising the feedforward FF and stretch REFLEX. This can be symbolically expressed as:

$$\text{COMMAND} = (\text{FF} + \text{REFLEX})(1 + \text{NOISE}) \quad (12)$$

In Section 3.3, the linear model of motor noise that we implement in simulation will be described in detail.

2.5 Learning Algorithm

The learning algorithm realizes *feedback error learning at the muscle level*. The idea is that muscle reflex is representative of the force to move the arm along the desired movement. Therefore it can be incorporated into the feedforward command for the next trial to provide the force necessary to move the arm along the desired movement. While this is similar to conventional feedback error learning or iterative control in joint space (Kawato *et al* 1987, Bien and Xu 1998, Burdet *et al* 1998), a fundamental difference appears when consecutive trials oscillate around the mean trajectory as typically occurring in unstable situations (Osu *et al* 2003, Burdet *et al* 2003).

To provide an illustrative example of how muscle FEL stabilises unstable dynamics, let us consider the activities of biarticular muscles during multijoint arm movement in an unstable interaction. The interaction causes consecutive trajectories to alternate on either side of the mean trajectory (Fig. 5). When the movement is initially to the right, the biarticular flexor is stretched and experiences an increase of activity due to muscle elasticity and reflex. If we neglect the cross reflex in this example, then the biarticular extensor does not increase activity since it is shortened. In the subsequent trial, the feedforward for the flexor is increased due to muscle FEL, However, in the given unstable

interaction, this results in a movement to the left, eliciting a reflex increase of activity in the extensor that is in turn incorporated into the feedforward of the extensor. In addition to learning a mean force of zero, as in the case of conventional (joint) FEL, muscle FEL also leads to a build-up of cocontraction of agonist and antagonist muscles. This provides an increase of arm impedance, as shown in (11) and Table 1, that gradually compensates for the instability.

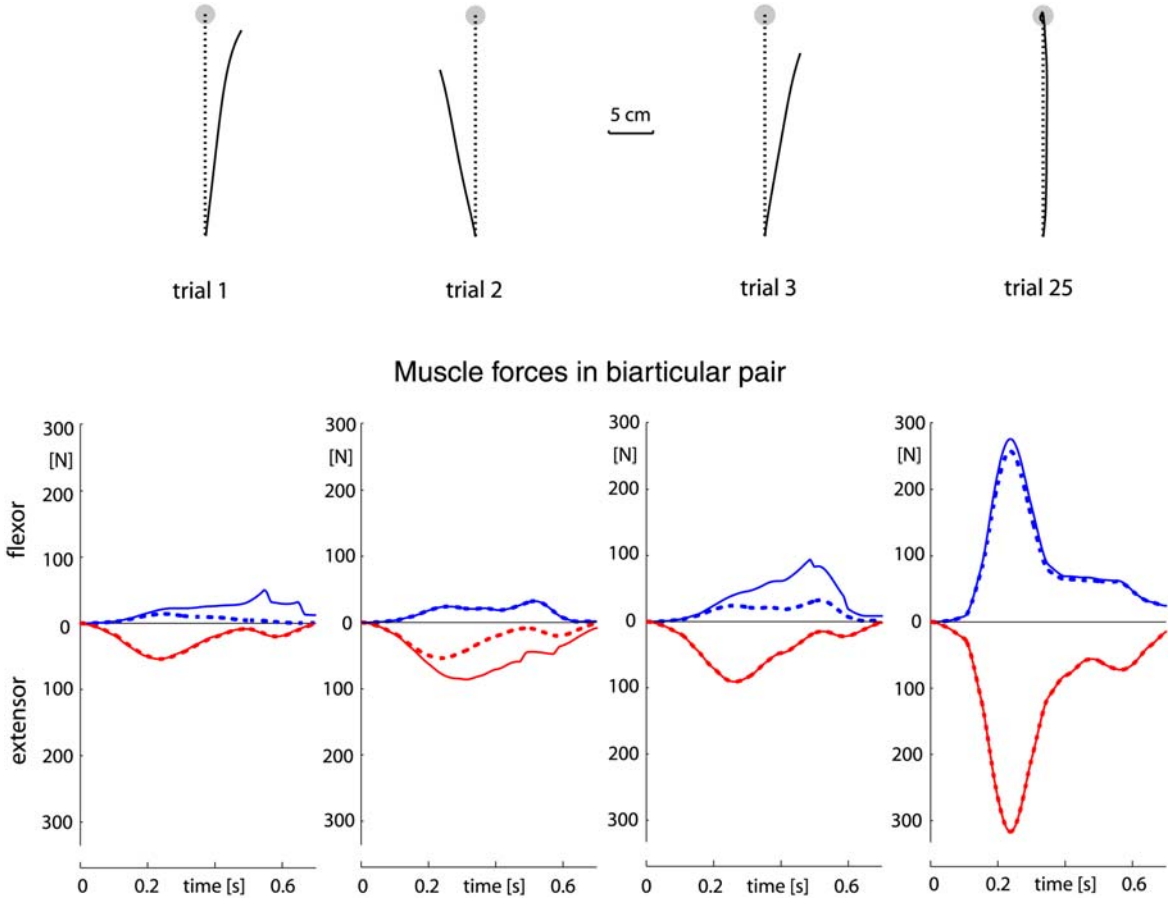

Fig. 5 Feedback error learning at the muscle level can stabilize unstable dynamics. Movements in DF for initial trials and after adaptation are shown in the top row. Centerline is shown dotted. Biarticular muscle forces are shown in the bottom row, with dotted lines representing the feedforward component and solid lines representing sum of feedforward and feedback components. Movements alternating left and right of the centerline result in a buildup of cocontraction in both muscles, hence increasing impedance. Results are simulated.

Cocontraction is further increased with the inclusion of the cross term in reflexes, as described in (9). To remove superfluous cocontraction during adaptation, muscle deactivation is necessary. Thus the learning algorithm can be formulated as:

$$m^{k+1}(t) \equiv m^{k}(t) - \gamma(t) + \alpha\, r(t+\varphi) \qquad (14)$$

The superscript ^{k} denotes the number of elapsed learning trials, m is the feedforward muscle tension, γ the deactivation term, r the reflex and α the learning factor. The phase advance φ in the feedforward update is taken to be equal to the reflex delay ϕ in (10).

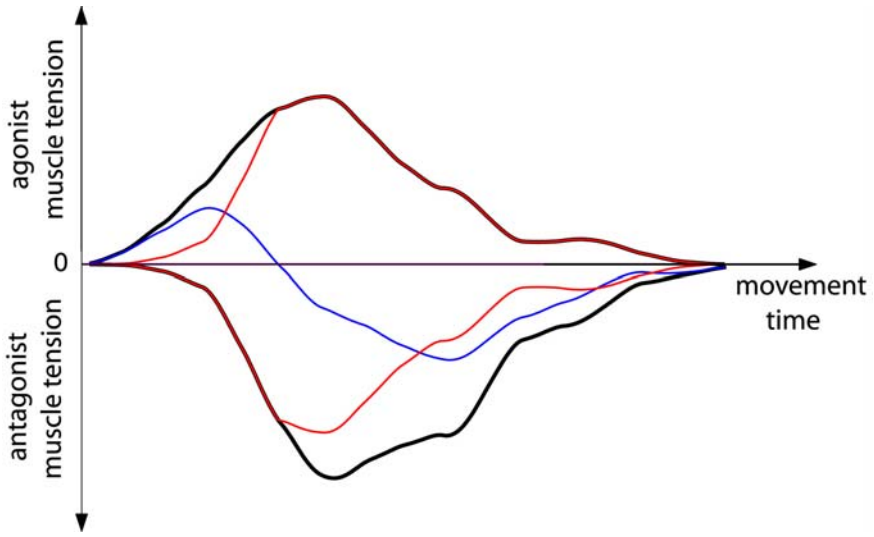

Fig. 6 Reciprocal activation and cocontraction in agonist-antagonist muscle pair. The feedforward muscle tension (black) is composed of reciprocal activation (blue) and cocontraction (red). Reciprocal activation is defined by the difference of muscle forces i.e. (m_a-m_{aa}), and cocontraction by the common force in both muscles i.e. ½ (m_a+m_{aa}-|m_a-m_{aa}|).

The results of Section 5 show that this simple algorithm concurrently learns the inverse dynamics and the increase in impedance required for stable task performance in unstable or stable dynamics. For equal moment arms ρ of the agonist and antagonist on the same joint, the amount of cocontraction v and feedforward torque u (Fig. 6) are:

$$v = \tfrac{1}{2}(m_a + m_{aa} - |m_a - m_{aa}|) \qquad (15)$$

$$u^{k+1} = \rho\,(m_a^{k+1} - m_{aa}^{k+1})$$

$$= \rho\,[m_a^{k} - m_{aa}^{k} + \alpha\,(r_a - r_{aa})]$$

$$= u^{k} + \alpha\,\rho\,(r_a - r_{aa})$$

$$= u^{k} + \alpha\,\tau_r$$

It can be seen that the torque is updated in a manner similar to the classical feedback error learning algorithm (Kawato *et al* 1987, Burdet *et al* 1998), i.e. the reflex torque τ_r serves as the teacher signal to update the feedforward torque, leading to the acquisition of an inverse dynamics model (Slotine 1991).

2.6 Learning Factor

All muscles have the same learning factor α that increases with the kinematic stretch error of muscles within the movement. In particular, we consider the time-averaged stretch error of the agonist and antagonist within each muscle pair, and then take the maximum amongst the three muscle pairs:

$$e^{k} \equiv (1/T)\,\max_j \int_0^T [\Delta\lambda_a^{k}(t) + \Delta\lambda_{aa}^{k}(t)]_j\,dt \qquad (16)$$

T is the movement time, k is the trial number, and j is the muscle pair index. Taking the maximum ensures a sensitive trigger condition for learning.

This will derive a single measure of stretch error $\bar{e}$ for each movement that in turn determines the learning factor α

$$\bar{e}^{k} \equiv (1-\eta)\,\bar{e}^{k-1} + \eta\,e^{k} \qquad (17)$$

$$\alpha \equiv \tfrac{1}{2}\,\alpha_0[1 + \tanh(\sigma(\bar{e}^{k} - \varepsilon))] \qquad (18)$$

Equation (17) is necessary to average the stretch error over previous trials, otherwise the error signal is very noisy due to movement variability. The threshold error ε in (18) prevents an unbounded increase of impedance to eliminate motion variability. An alternative would be to implement a constant learning factor and a threshold in the reflex, so that when kinematic error is within normal motion variability, there will be no reflex action and hence no learning. However, the reflex error signal can be very noisy. Without any averaging of inter-trial errors, learning performance may not be satisfactory.

2.7 Anisotropic Impedance Learning

The following two-step adaptation strategy results in anisotropic impedance along the direction of instability, as was observed in experiments (Burdet at al 2001A).

Step 1. Through muscle FEL, an imposed deviation in a (Cartesian) direction induces an increase of endpoint stiffness in about the same direction.

Step 2. Selective deactivation is performed to minimize superfluous muscle cocontraction not required for task stabilization.

Step 1: Increase of endpoint stiffness in the direction of imposed deviation

The increase of stiffness due to the shoulder and elbow single-joint muscles is always in the same direction independent of the moment arms. On the other hand, the direction of stiffness increase resulting from cocontraction of biarticular muscles depends on the ratio of the moment arms at the two joints spanned by the muscles. To investigate whether the direction of stiffness change is correlated with the direction of the deviation, we compute the change of endpoint stiffness $\Delta\mathbf{K}_x$ corresponding to the trajectory deviation $\Delta\mathbf{x}$. The

variables used here are defined in Section 2.2. From Table 1, the muscle stretch corresponding to deviation $\Delta\mathbf{x}$ is

$$\Delta\boldsymbol{\lambda} = \mathbf{J}_m\mathbf{J}^{-1}\Delta\mathbf{x} \; . \tag{19}$$

Feedback error learning in muscle space gives an increase of muscle force proportional to the imposed muscle stretch:

$$\Delta\mathbf{m} = \mathrm{diag}[\alpha_1, \alpha_2, .. \alpha_6]\; \Delta\boldsymbol{\lambda} = \mathrm{diag}[\alpha_1, \alpha_2, .. \alpha_6]\; \mathbf{J}_m\mathbf{J}^{-1}\Delta\mathbf{x} \tag{20}$$

The associated modulation of stiffness is equal to $\mathrm{diag}[\kappa_1\Delta\mathbf{m}]$ in muscle space. The change in endpoint stiffness resulting from a deviation $\Delta\mathbf{x}$ is expressed as

$$\Delta\mathbf{K}_x = (\mathbf{J}_m\mathbf{J}^{-1})^T\, \mathrm{diag}(\kappa_1\, \Delta\mathbf{m})\, (\mathbf{J}_m\mathbf{J}^{-1}) \tag{21}$$

The geometry of stiffness increase depends on the learning factors $\alpha_1, \alpha_2, .. \alpha_6$ and on $\mathbf{J}_m$, i.e. the moment arms. In order to visualize endpoint stiffness in the Cartesian workspace, we represent stiffness as an ellipse, which is obtained by plotting the coordinates of the force vectors $\mathbf{F}_s(\theta)$ generated by a unit rotating input displacement vector. The stiffness ellipse is represented as:

$$\mathbf{F}_s(\theta) = \mathbf{K}_x \begin{bmatrix} \cos\theta \\ \sin\theta \end{bmatrix} \qquad 0 < \theta < 2\pi \tag{22}$$

It can be seen that with all the learning factors set to 1, and moment arms identical, the increase of endpoint stiffness induced by a deviation $\Delta\mathbf{x} = (1,0)$ is not in the same direction (Fig. 10). In our model, for simplicity, the learning factors are set equal, i.e. $\alpha \equiv \alpha_1 = \alpha_2 = \alpha_3 = \alpha_4 = \alpha_5 = \alpha_6$, and the moment arms are appropriately chosen to produce a stiffness change that is in the same direction as the imposed deviation. An alternative

would be to vary the learning factors. This would suggest the possibility that the CNS adaptively compensates for the inherent moment arms.

Step 2: Selective deactivation

Muscle FEL as described in (14) does not automatically produce the selective increase of impedance in the direction of instability as observed in (Burdet *et al* 2001A). Rather, superfluous increase of impedance is also produced in directions that are relatively stable. To remove superfluous impedance, anisotropic deactivation is required. This can be realized through a combination of two strategies:

i. An independent deactivation process where each muscle pair decreases activity relative to itself and independently of the other muscle pairs, realized by:

$$\gamma_i(t) = \gamma_0 \, v_i(t) \qquad (23)$$

where γ_0 represents the decay factor, and subscript $_i$ represents either shoulder, elbow or biarticular muscle pair.

The associated decrease in stiffness is isotropic and will not produce the elongated ellipses (Fig. 1E) observed in the experiment (Burdet *et al* 2001A).

ii. A homogenous deactivation process, where all muscles decrease activity by the same amount. One possibility is to consider the mean cocontraction level of all muscle pairs:

$$\gamma_i(t) = \gamma_0 \, [v_i(t)+v_{j1}(t)+v_{j2}(t)]/3 \qquad \text{where } j1, j2 \neq i \qquad (24)$$

The principle of this deactivation process is that the decrease of cocontraction in one muscle pair may 'diffuse' to the other muscle pairs. It can be easily shown that if

$v_i > \{v_{j1}, v_{j2}\}$

then

$\{\gamma_{j1}/v_{j1}, \gamma_{j2}/v_{j2}\} > \gamma_i/v_i$

meaning that the relative decay of muscle pairs j1 and j2 will be higher than that of muscle pair i. This diffusion results in anisotropic stiffness decrease by causing a faster deactivation in the muscle pairs with relatively smaller cocontraction level (winner-takes-all).

Combining these two strategies yields a more general form, where the relative rate of deactivation of the muscle pairs is determined by γ_1.

$$\gamma_i(t) = \gamma_0 [\gamma_1 v_i(t) + \tfrac{1}{2} (1-\gamma_1) v_{j1}(t) + \tfrac{1}{2} (1-\gamma_1) v_{j2}(t)] \quad (25)$$

where $\gamma_0 > 0$, $1/3 < \gamma_1 < 1$.

3 Implementation

Section 2 has generally described the dynamic equations of the model in terms of its parameters. To investigate the control and learning behavior resulting from these equations, and thereafter to evaluate the plausibility and robustness of the model, simulations need to be performed. In this chapter, we will look at the definition of the movement tasks to be simulated, as well as the issues in implementation, namely the algorithm for integrating the motion and the selection of parameters for muscle elasticity, reflex, noise and learning.

3.1 Simulation of Movement Tasks

The simulation of the learning model is based on experimental conditions similar to that in real experiments (Burdet *et al* 2001A, Franklin *et al* 2003A, Osu *et al* 2003, Franklin *et al* 2003B, Franklin *et al* 2002). This section defines the movement task, physical constraints, and environmental interactions in the computational experiment.

The start and target locations for simulated movements are at (x,y)=(0,0.31)m and (0,0.56)m respectively, with the coordinates relative to the shoulder joint. The movement is constrained such that shoulder and elbow movements are on the horizontal plane. Duration of movement is 600ms.

Before interaction with novel dynamics, the dynamics of null field movements are to be learnt. To do this, the muscle forces are first initialized from the feedforward joint torque by minimising the sum of squared muscle forces (Pedotti 1978, Collins 1995) i.e. $\mathbf{m}^T\mathbf{m}$. Then, the optimal muscle forces are modified through learning in 100 NF

movements. The mean muscle forces obtained over the last 20 trials are used as the feedforward command at the start of any novel dynamics learning.

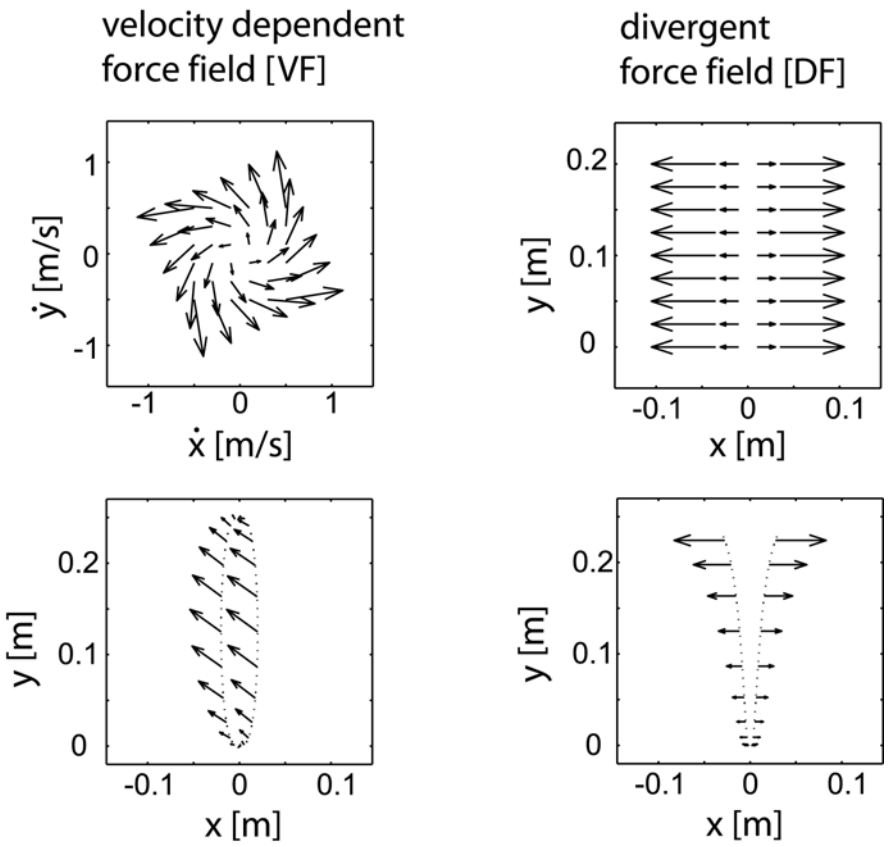

Fig. 7 Velocity-dependent field (VF) producing stable dynamics and diverging field (DF) producing unstable dynamics. *Top row*: Vector field of the external force as a function of hand velocity for VF and hand position for DF. *Bottom row*: External force experienced when movement trajectory deviates slightly left and right of the straight line along the y-axis.

The external force consists of not only the novel dynamics arising from interaction with the environment, but also the friction and inertia of the parallel link direct drive air and magnet floating manipulandum (PFM) used in (Burdet *et al* 2001A, Franklin *et al* 2003A, Osu *et al* 2003, Franklin *et al* 2003B, Franklin *et al* 2002). The PFM dynamics, with parameters identified by (Franklin 2002), are represented as:

$$\boldsymbol{\tau}_{PFM} = \mathbf{J}^{T}[\mathbf{M}\,\mathbf{a} + \mathbf{D}_{d}\,\mathbf{v} + \tanh(200\,\mathbf{D}_{s}\,\mathbf{v})] \qquad (26)$$

where $\mathbf{M}=\begin{bmatrix}1.516 & 0\\ 0 & 1.404\end{bmatrix}$, $\mathbf{D}_d=\begin{bmatrix}10.247 & 0\\ 0 & 7.592\end{bmatrix}$, $\mathbf{D}_s=\begin{bmatrix}0.102 & 0\\ 0 & 0.356\end{bmatrix}$; $\mathbf{v}$ and $\mathbf{a}$ are the hand velocity and acceleration respectively. The static friction dynamics are smoothened by the hyperbolic tangent function.

Movements are performed in novel dynamics and adaptation is allowed to take place for 100 learning trials. Two types of novel dynamics, representative of stable and unstable interactions, are simulated:

i. Velocity-Dependent Field (VF)

$$\mathbf{F}_{VF}=\begin{bmatrix}-13 & 18\\ -18 & -13\end{bmatrix}\mathbf{v} \quad (27)$$

With this force field, a stable interaction with the arm is produced, as can be inferred from the eigenvalues of the linearized coupled system. Despite different trajectories to the left and right of the straight line along the y-axis, the external forces acting on the hand are similar (Fig. 7), and hence reproducible. The force field is shut down when the hand is within 0.0125m radius of the target.

ii. Position-dependent Diverging Field (DF)

$$\mathbf{F}_{DF} = (-350x, 0) \quad (28)$$

The DF produces a force proportional to the hand position as measured from the y-axis, resulting in an unstable interaction with the arm. The force field is shut down when the hand is within 0.0125m radius of the target. The net stiffness, defined by the sum of the negative environmental stiffness and the endpoint stiffness of the arm, has negative eigenvalues before adaptation, leading to instability when there is a perturbation. As a result, movements diverge irretrievably (Fig. 7).

To prevent "breaking the arm", there is a boundary 4cm from the centerline and on both sides. When the hand reaches this boundary, the force field is shut down and a restoring force **F**=(40 $\dot{x}$, 0) is applied on the hand for the duration of which the hand is outside the boundary. When the hand falls within the boundary again, it is allowed to move freely to the target.

3.2 Motion Integration

The algorithm for motion integration is shown in the flowchart of Fig. 8. Anthropometrical data for the segments (Diffrient *et al* 1978), used in the motion simulations, are shown in Table 2.

The planned trajectory in Cartesian space, x_d, is defined as the mean NF trajectory measured in (Burdet *et al* 2001A). During the computation of the mean trajectory, a velocity threshold of 0.001ms^{-1} is used to define the start of each experimental movement. The planned trajectory in joint coordinates q_d is realized via inverse kinematics (Appendix A).

Table 2 Anthropometrical data for arm segments

	Mass (kg)	Length (m)	Center of mass relative to proximal joint (m)	Mass moment of inertia (kg m^2)
Upper arm	1.93	0.29	0.165	0.0141
Forearm	1.52	0.34	0.19	0.0188

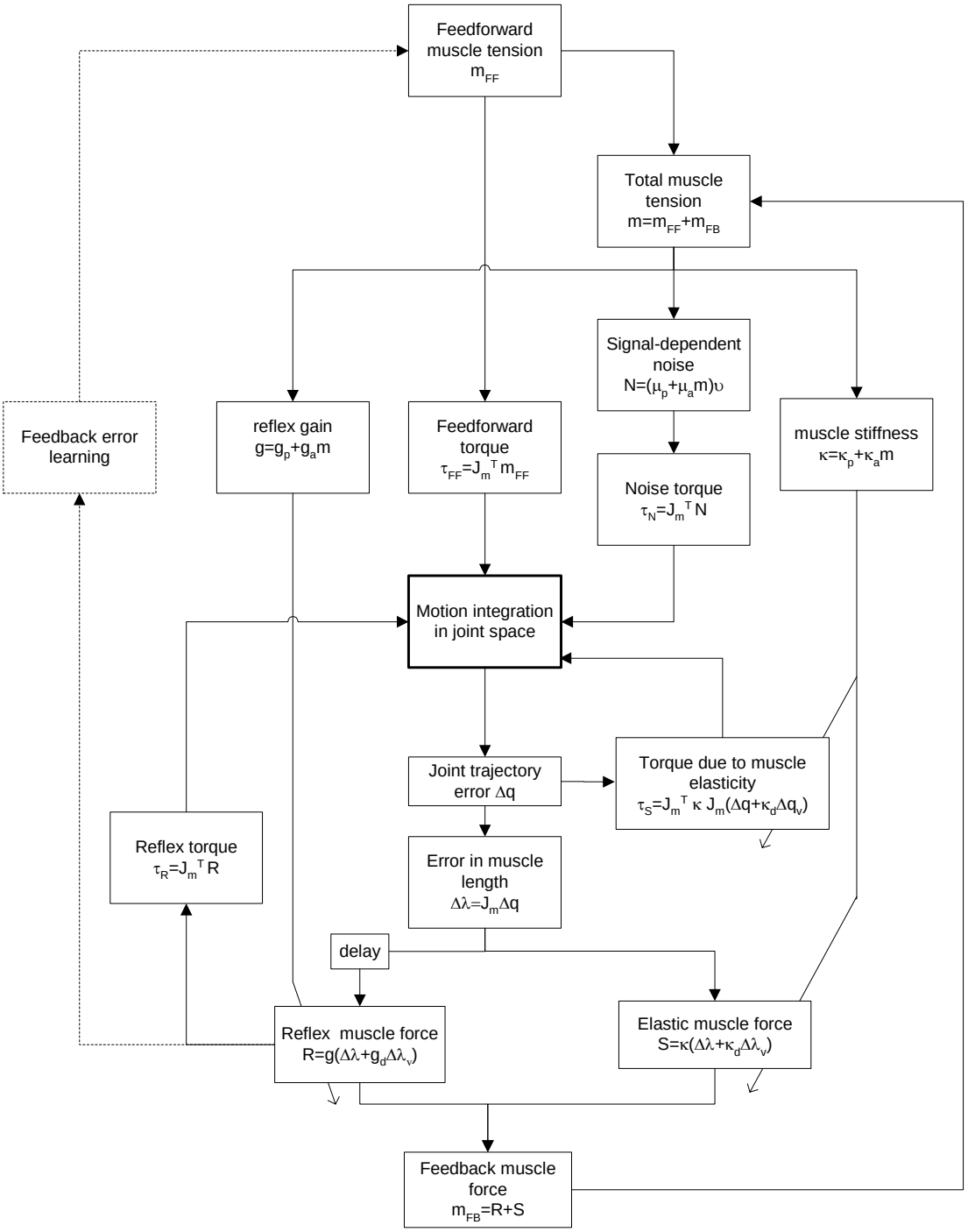

Fig. 8 Flowchart for motion integration algorithm. Motion integration is in joint space, with the inputs at any time being the feedforward torque, reflex torque, torque due to muscle elastic response, torque due to motor noise and external torque (not shown). Any error in movement resulting from this interaction of dynamics elicits changes in muscle forces (via reflexes and muscle elasticity) and hence affects the movement at the next time instant. The reflex of the movement is used to modulate the feedforward of the successive movement i.e. feedback error learning, shown in dotted line.

In order to curb oscillations after reaching the target, a high damping force is implemented when the y-displacement is more than 0.245m (y-displacement of the target is 0.25m).

$$\boldsymbol{\tau}_v = \mathbf{J}^T(-50\mathbf{v}) \tag{29}$$

To obtain the movement resulting from the interaction of the arm and the environment, (5) is Euler integrated at 500Hz:

$$\mathbf{q}_a(t) = \boldsymbol{\Gamma}(\mathbf{q}(t-\Delta t), \mathbf{q}_v(t-\Delta t), \mathbf{m}(t-\Delta t)) \tag{30}$$

$$\mathbf{q}_v(t) = \mathbf{q}_v(t-\Delta t) + \mathbf{q}_a(t)\,\Delta t$$

$$\mathbf{q}(t) = \mathbf{q}(t-\Delta t) + \mathbf{q}_v(t-\Delta t)\,\Delta t + \tfrac{1}{2}\,\mathbf{q}_a(t)\,\Delta t^2$$

where t is the movement time, Δt the sampling time, and $\boldsymbol{\Gamma}$ the dynamics of interaction depending on the joint position $\mathbf{q}$, joint velocity $\mathbf{q}_v$ and muscle activity $\mathbf{m}$ of the previous time.

The simulations are performed in Matlab 6.5 under Windows environment.

3.3 Reflex, Impedance and Noise Parameters

The interplay of reflex, impedance and noise in the motor control system produces the deviation in movements that we observe. We want to use reflex, impedance and noise parameters corresponding to experimental values and producing deviation similar to that of real movements. The dynamic equations and default parameter values used in simulation are listed in Appendix C.

3.3.1 Reflex and Impedance

The learning controller described in Section 2.5 corresponds to a nonlinear adaptive controller in muscle space, with the reflex and impedance depending on the proportional and derivative terms of the imposed muscle stretch. It has been demonstrated mathematically that nonlinear adaptive controllers converge with any positive proportional or derivative term of the error (Bayard and Wen 1998), suggesting that in our case convergence should also occur with any positive proportional or derivative term of the stretch. Our simulations confirmed this. However, a zero derivative term resulted in slightly oscillating trajectories different from real movements. The selected proportional and derivative terms are plausible as long as they produce movements that are kinematically similar to real movements.

In the impedance modeling, the following stiffness parameters are selected: κ_d= 1/12, κ_0=2844Nm^{-1}, κ_1=0.035m^{-1}, producing stiffness ellipse in NF similar to what is measured in experiments (Franklin *et al* 2003, Burdet *et al* 2001A, Gomi and Kawato 1997).

In the reflex modeling, the strength of the cross reflex, β, is estimated to be 0.4 (Franklin 2003B) and the reflex gains are selected as: g_0=114Nm^{-1}, g_1=0.035m^{-1}, g_d= 2. Only long latency reflexes with a fixed delay ϕ=100ms are incorporated, because short latency reflexes are negligible for long-duration, low frequency perturbations (Lee and Tatton 1982), which characterise the task interactions of (Burdet *et al* 2001A). The onset of long latency EMG response typically is delayed by 55-65ms from the onset of perturbation. Considering that we are working with muscle forces and not EMG, there is an additional latency of 25-50ms to account for excitation-contraction coupling and time

to reach maximum muscle contraction. The sensitivity of the model to the reflex delay will be analyzed in Section 4.2.1.

The above selection of parameters for reflex and impedance ensured a reflex contribution of 20-35% of total restoring response, similar to the physiological range of 18-44% (Carter *et al* 1990).

3.3.2 Noise

Noise is realized as Brownian motion. This produces similar motion variability as in real movements. It is implemented in the following way. First, Gaussian noise is generated at 500Hz, using the in-built Matlab random generator *randn* that is based on the Ziggurat Algorithm (Marsuglia and Tsang 1984). The high frequency content is then attenuated using a fifth order low-pass Butterworth filter with a cutoff frequency of 2Hz. Finally the delay (of 80ms, as we find through cross-correlation) inherent in this filter is compensated for, to obtain a noise series $\{\nu(t)\}$. The noise for each muscle is then computed as

$$n(t) = (\mu_0 + \mu_1 m(t))\,\nu(t) \tag{31}$$

with μ_0 =0.0725 and μ_1 =6.5.

3.3.3 Motion Variability

To evaluate the selection of parameters for reflex, impedance and noise, inter-trial variability of simulated and real motion are compared. (Fig. 9A) shows that the histograms of absolute hand path error, defined by

$$E_p = \int_o^T |x(t)\|\dot{y}|(t)\,dt \tag{32}$$

with *T* as the movement time, are similar between simulated and real NF movements. Besides inter-trial variability, positional variance within movement is also compared (Fig. 9B). There is a close match of positional variance for movement time up to about 700ms, after which the variance for real movements drops sharply. Since 700ms corresponds to the mean time when the hand reaches the target, the drop in variability of real movements can be explained by visual/voluntary correction, which is significant in the proximity of the target for reaching tasks. Because the model does not incorporate visual/voluntary feedback, it is expected that the variance of simulated movements is higher after 700ms. Nevertheless, this late phase of movement does not significantly affect the adaptation. On the whole, the above selection of reflex, impedance and noise parameters successfully produces motion variability similar to that of real movements.

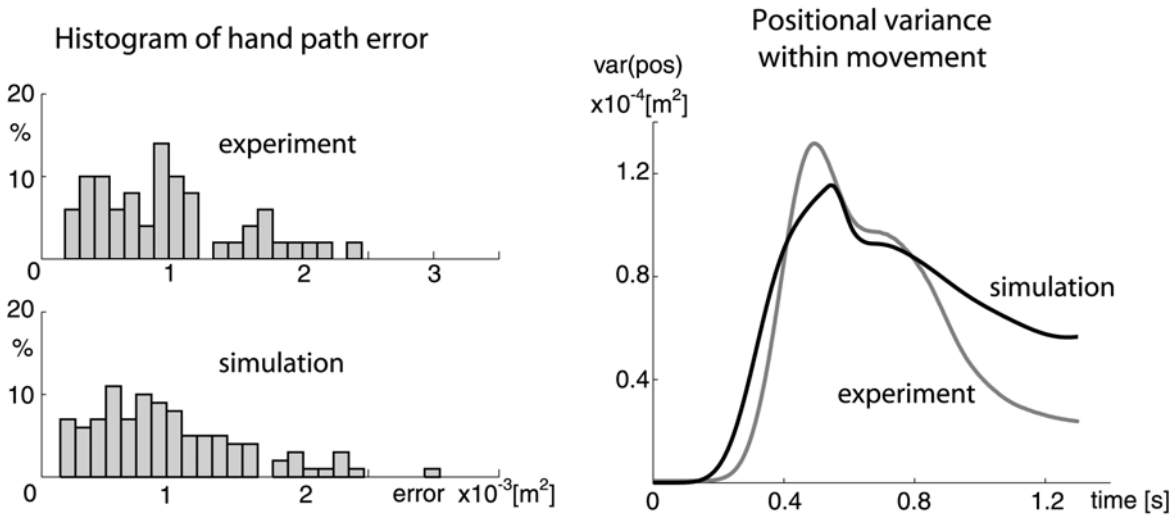

Fig. 9 Histograms of absolute hand path error and positional variances during simulated and real NF movements over 50 trials.

3.4 Learning Parameters

3.4.1 Moment Arms

Equal moment arms are taken for each pair of agonist and antagonist muscles acting at a joint. For the biarticular muscles, the moment arm ratio between the shoulder and elbow joints is selected such that a deviation $\Delta\mathbf{x}$ = (1,0) produces a stiffness increase approximately in the same direction. This condition can be obtained with a ratio between 1.3 and 1.5, of which we select 1.3. Fig. 10 shows how the different muscle pairs can modify endpoint stiffness. The increase of activity in each muscle pair causes endpoint stiffness to increase in a fixed direction by a magnitude depending on the moment arm. To obtain NF stiffness geometry as measured in experiment (Fig. 1E), the moment arms corresponding to the three muscles pairs are tuned. The matrix of moment arms is represented as:

$$\mathbf{J}_{\mathrm{m}} = \begin{bmatrix} 0.028 & -0.028 & 0 & 0 & 0.044 & -0.044 \\ 0 & 0 & 0.017 & -0.017 & 0.0338 & -0.0338 \end{bmatrix}^{\mathrm{T}} \mathrm{m} \qquad (33)$$

3.4.2 Deactivation

To obtain anisotropic stiffness modulation similar to what was measured in the experiments, the parameters γ_0 =0.04 and γ_1=0.7 are used in (24), with the condition:

$$\gamma(\mathrm{t}) = \begin{cases} v(\mathrm{t}) & \text{for } \gamma(\mathrm{t}) > v(\mathrm{t}) \\ \gamma(\mathrm{t}) & \text{otherwise} \end{cases} \qquad (34)$$

This ensures that only the built-up co-contraction, but not the learnt torque, decreases and in turn $m_a \geq 0$ and $m_{aa} \geq 0$.

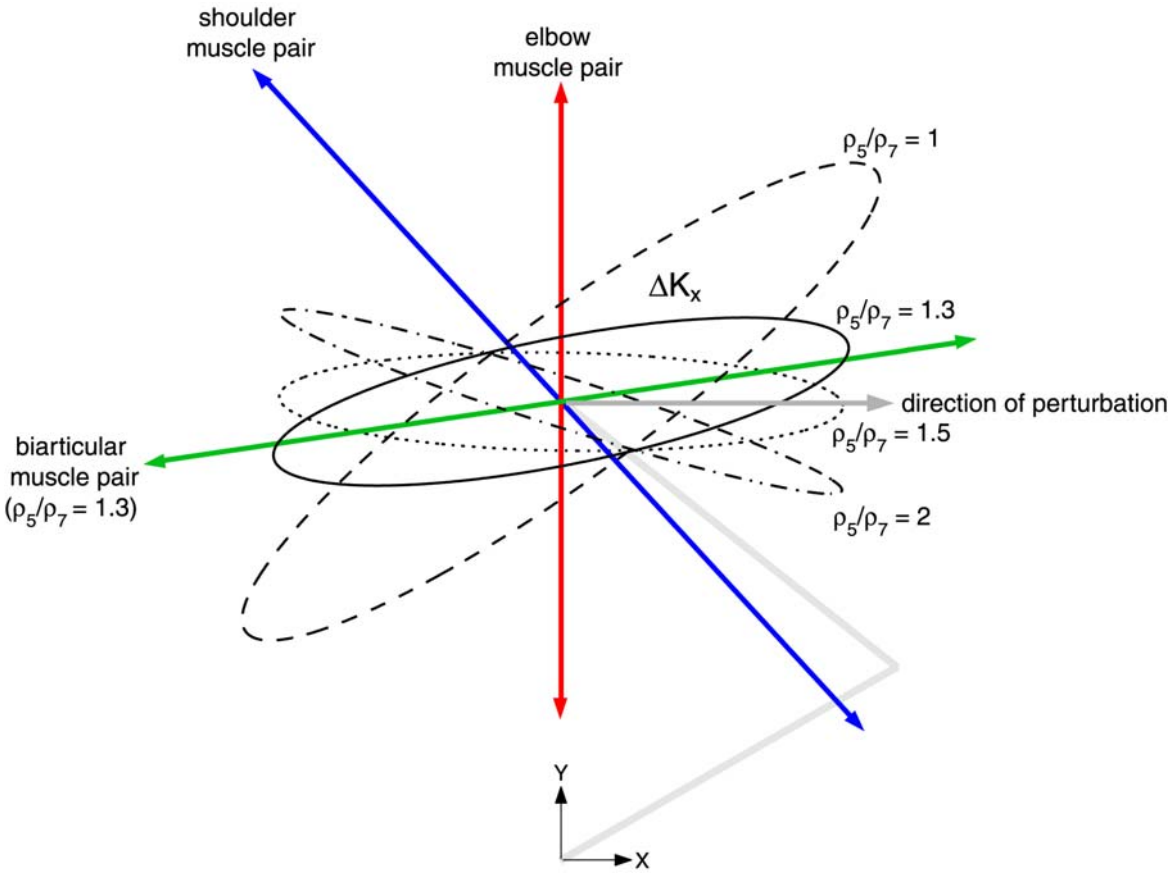

Fig. 10 Relationship between endpoint stiffness geometry, muscle pairs cocontraction, and moment arms. Each of the bold lines represent the axis along which the endpoint stiffness changes when the muscle stiffness or the moment arms of the pair changes. We term this the "muscle pair stiffness axis". With the endpoint perturbed in the $(1,0)^T$ direction (perpendicular to the movement), stiffness change ellipses ΔK_x resulting from feedback error learning are plotted for different ratios of moment arms of the biarticular muscle pair. Ratio is defined as ratio of moment arm spanning the shoulder to moment arm spanning the elbow. Ratios between 1.3 and 1.7 produce elongation of the stiffness ellipse roughly in the direction of the perturbation.

3.4.3 Learning Factor

In the computation of the learning factor α from (17), the threshold error $\varepsilon = 5.65 \times 10^{-4}$m is selected to give a low α in NF movements such that there is minimal learning. $\sigma = 5500 \text{m}^{-1}$ is selected such that there is adequate learning (high α) in the initial adaptation to novel dynamics and minimal learning (low α) after adaptation.

The parameter η is given by:

$$\eta(k) = \begin{cases} 2/5 & \text{for } k<=8 \\ 1/8 & \text{for } k>8 \end{cases} \quad (35)$$

so that the initial learning will be more reactive to large changes in the kinematic error that characterize novel dynamics. After adaptation, the response to changes in error is more damped.

4 Results

4.1 Adaptation to VF and DF

The simulated hand trajectories, muscle activity and stiffness, during adaptation in both VF and DF, are highly consistent with experimental data (Burdet *et al* 2001A, Franklin *et al* 2003A, Osu *et al* 2003, Franklin *et al* 2003B) that are shown in Figs.1 and 2.

The simulation results for adaptation to VF are shown in Fig. 11. The *before effects*, corresponding to movements subjected to the unexpected onset of the force field, show the effect of the force field before adaptation takes place. Like the before effects, the initial learning trials are perturbed to the left, but with a fast reduction of kinematic error over trials due to adaptation. Movements become fairly straight within 10 trials. The *after effects*, corresponding to adapted movements subjected to the unexpected shutdown of the force field, deviate to the right forming a mirror image of the before effects. This shows that an inverse dynamics model of VF has been acquired.

The model predicts a sharp increase of muscle activity in the initial trials followed by the onset of gradual reduction after about ten trials. Due to the cross reflexes, there is an increase of flexor muscle activity in the initial learning phase even though the flexor muscles are not stretched.

After adaptation, there is a distinct increase of reciprocal activation in the extensor muscles, corresponding to the acquired inverse dynamics of VF. This can be distinctly identified in the shoulder muscles, which are primarily responsible for producing the necessary forces to compensate for VF. Cocontraction increases sharply in the initial 10 trials and then undergoes a gradual decrease for all muscle pairs. Because of the relatively

larger activity in the shoulder muscles, the endpoint stiffness is larger in the direction of the shoulder pair stiffness axis (see Fig. 10).

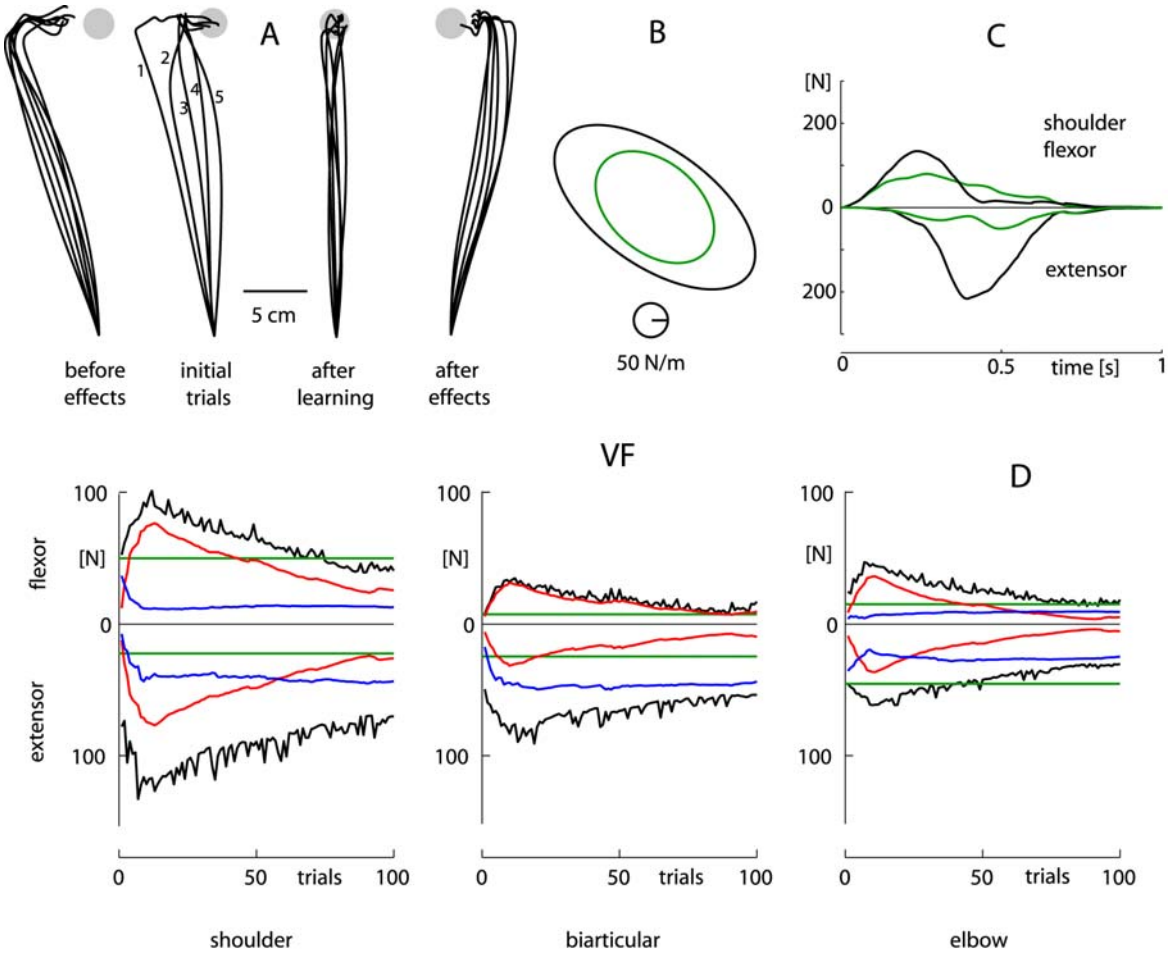

Fig. 11 Simulated adaptation to VF. *A*: Hand trajectories in initial and final adaptation, as well as after effects of adaptation. *B*: Adapted endpoint stiffness (black) and NF stiffness (green). *C*: Shoulder muscles activation in NF (green) and adapted (black) movements. *D*: Evolution of mean muscle forces (black) over 100 learning trials in VF. Green lines represent the mean muscle force levels in NF movements. Blue and red represent mean levels of reciprocal activation and cocontraction respectively.

Fig. 12 shows the simulated results for adaptation to DF. Initial movements, like before effects, diverge in both left and right directions, but after about 25 trials, movements are straight. After effects are also straight, showing that no meaningful inverse dynamics model of DF is learnt. This is expected since inverse dynamics models are only

meaningful when the dynamics to be learnt are reproducible, which is not the case for DF. The after effects also show significantly less deviation from the centerline as compared to NF movements, due to the increase of impedance in the x-direction. Relative to NF stiffness, the DF stiffness after adaptation is elongated in the direction of instability.

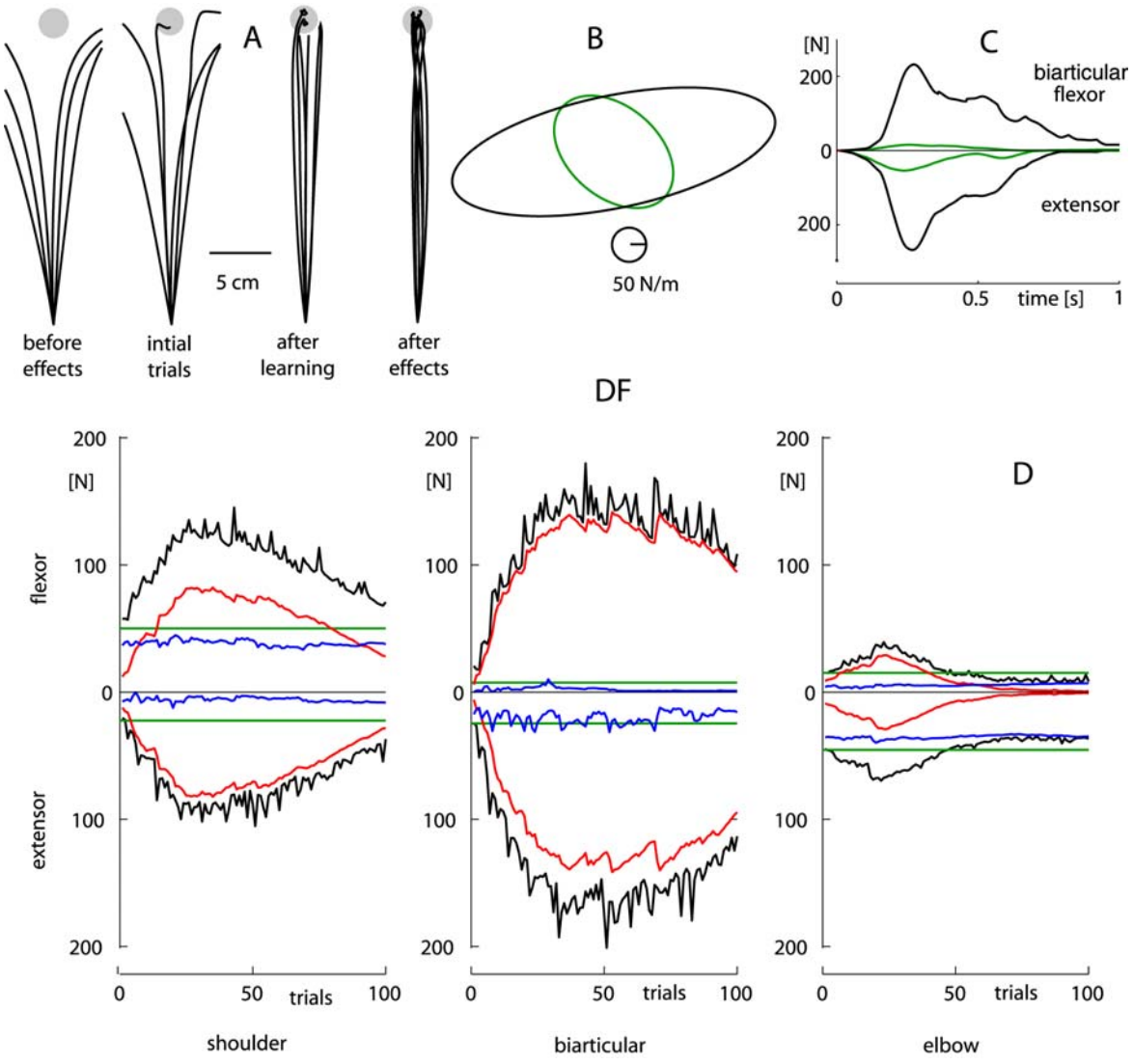

Fig. 12 Simulated adaptation to DF. *A*: Hand trajectories in initial and final adaptation, as well as after effects of adaptation. *B*: Adapted endpoint stiffness (black) and NF stiffness (green). *C*: Biarticular muscles activation in NF (green) and adapted (black) movements. *D*: Evolution of mean muscle forces (black) over 100 learning trials in DF. Green lines represent the mean muscle force levels in NF movements. Blue and red represent mean levels of reciprocal activation and cocontraction respectively.

There is a substantial increase in both flexor and extensor muscles after adaptation to DF, in contrast to the case of VF, which produced an increase only in the extensor muscles. Throughout adaptation to DF, reciprocal activation fluctuates at the same level but cocontraction undergoes a rapid initial increase in all muscle pairs followed by a gradual decrease after motion kinematic error is reduced (about 30 trials). Using (19), it can be shown that in DF, the biarticular muscles experience the maximal imposed stretch, followed by the shoulder muscles. The elbow muscles are hardly stretched. Following feedback error learning at the muscle level, the biarticular, shoulder and elbow muscles build up levels of cocontraction forces proportional to their respective stretch.

To visualize how endpoint stiffness changes throughout learning, stiffness ellipses are plotted after every 20 trials (Fig. 13A). In the initial learning phase (<20 trials), stiffness is large and relatively elongated in the direction of instability. Subsequently it undergoes an isomorphic decrease of size. The stiffness components in the stiffness matrix

$$\mathbf{K}_x = \begin{bmatrix} K_{xx} & K_{xy} \\ K_{xy} & K_{yy} \end{bmatrix}$$

are also plotted against learning trials (Fig. 13B). For DF, there is a significant increase of K_{xx} to counteract the instability in the x-direction, and a superfluous increase of K_{yy} that is removed by 100 trials.

In concurrence with impedance, the inverse dynamic model (IDM) of the environment changes throughout the learning (Fig. 13C). Here, we represent it in terms of feedforward joint torque. During adaptation to VF, there is a progressive increase of shoulder and elbow extensor torques, as the IDM is being learnt. After adaptation, the

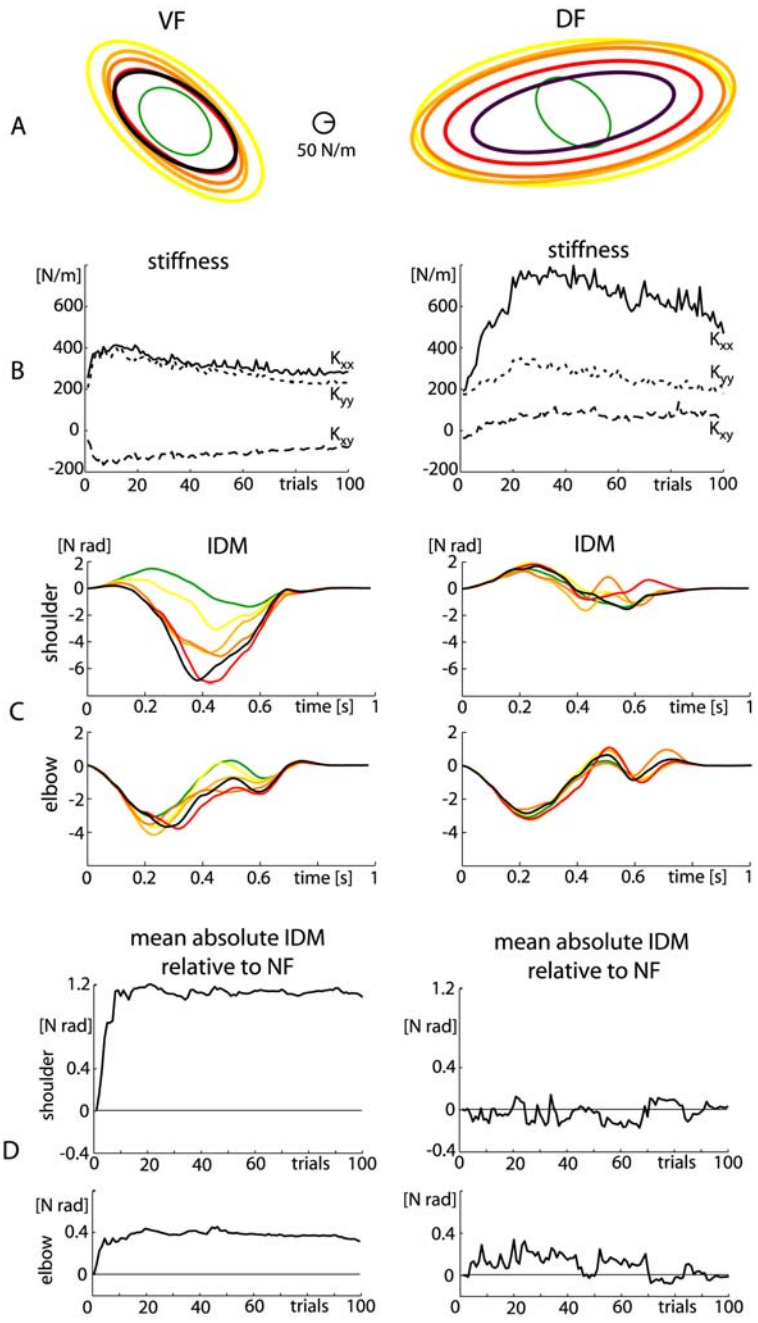

Fig. 13 Evolution of endpoint stiffness and inverse dynamics model (IDM). *A*: Stiffness ellipses are plotted at intervals of 20 trials during adaptation, with increasing color tone corresponding to increasing number of trials. The NF ellipse is shown in green. *B*: Endpoint stiffness is defined as $\mathbf{K}_x=\begin{bmatrix} K_{xx} & K_{xy} \\ K_{xy} & K_{yy} \end{bmatrix}$. The solid, dashed and dotted lines represent K_{xx}, K_{xy} and K_{yy} components respectively. *C*: The IDM waveform in joint space is shown for trials {2, 4, 6, 50, 100} during adaptation. Color tones from yellow to red correspond to increasing trial numbers. Green corresponds to the mean IDM in NF. *D*: The IDM waveform for each trial is rectified and averaged over movement time to obtain the mean absolute IDM. The difference between the mean absolute IDM in the force field and in NF is plotted over learning trials.

IDM corresponds to VF dynamics. Adaptation to DF yields a different behavior, producing an IDM that consistently fluctuates about the mean level even after a large number of trials. This is because the movements in DF tend to oscillate about the mean trajectory. To view the change in the level of IDM over trials, we take the mean of absolute IDM torque over movement time for each trial relative to the NF (Fig. 13D). The mean absolute IDM increases and converges smoothly within 10 learning trials in VF, in contrast to the fluctuations about a constant level in DF. These results show that while IDM learning compensates for stable dynamics, it is ineffective for adapting to unstable dynamics.

To investigate how the level of instability affects endpoint stiffness predicted by the model, we simulate adaptation to DF of different strengths. The external force is defined by

$$\begin{bmatrix} F_x \\ F_y \end{bmatrix} = -\kappa_e \begin{bmatrix} x \\ 0 \end{bmatrix}$$

where κ_e denotes the strength of the field, with values of 200N/m, 300N/m, 400N/m and 500N/m. Fig. 14 shows that as instability is increased along the x-direction, the adapted stiffness becomes increasingly elongated in the direction of instability with very minimal increase in the other directions. Hence the model has the property of producing the minimal stability margin needed to compensate for externally imposed instability. This is consistent with the experimental results of (Franklin *et al* 2003C), which suggests that the CNS employs a similar strategy minimizing metabolic cost when adapting to unstable dynamics.

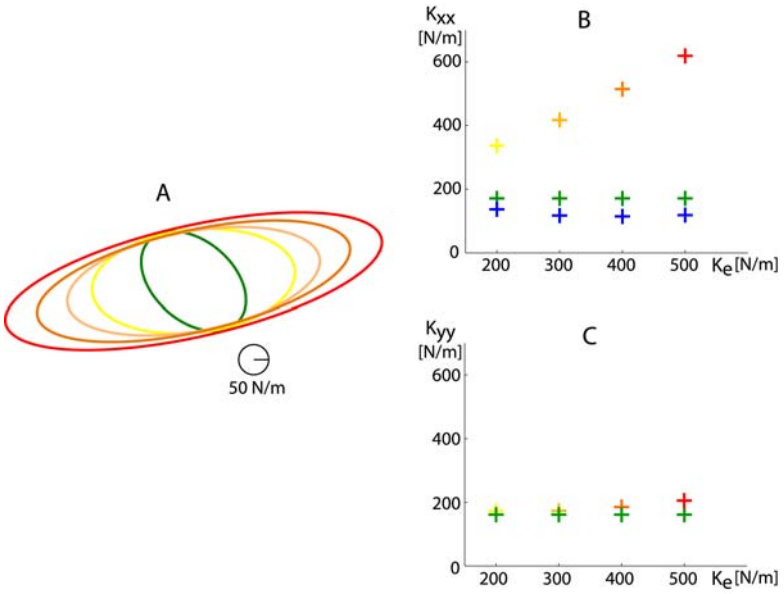

Fig. 14 Stiffness adaptation to DF of different strengths, namely 200N/m (yellow), 300N/m (orange), 400N/m (brown) and 500N/m (red). The NF stiffness is shown in green. *A*: Stiffness ellipses after adaptation. *B*: Stiffness component in the x-direction after adaptation. The net stiffness (i.e. the difference between the adapted stiffness and the environmental stiffness) in the x-direction is shown in blue. *C*: Stiffness component in the y-direction after adaptation.

4.2 Sensitivity to parameters

This section examines the sensitivity of the model's behavior to changes in parameters. The model's parameters can be categorized into three distinct groups: i) anthropometric parameters of the rigid-body model; ii) parameters influencing the control during movement; and iii) learning parameters. The sensitivity to the rigid-body parameters is not investigated, as the control depends smoothly and slowly on them and the performance do not vary with them.

4.2.1 Sensitivity to control parameters

As can be seen in Fig. 15, motion stability and learning are relatively insensitive to even a large delay in reflex. This is due to the fact that the feedforward learned in consecutive trials produces the motion dynamics, thus the feedback only needs to provide stability to

unexpected perturbations (Burdet *et al* 2003). When the delay is below about 100ms, there is almost no effect on learning and control. When the delay is larger, the control deteriorates slightly and requires a small increase of impedance for stability.

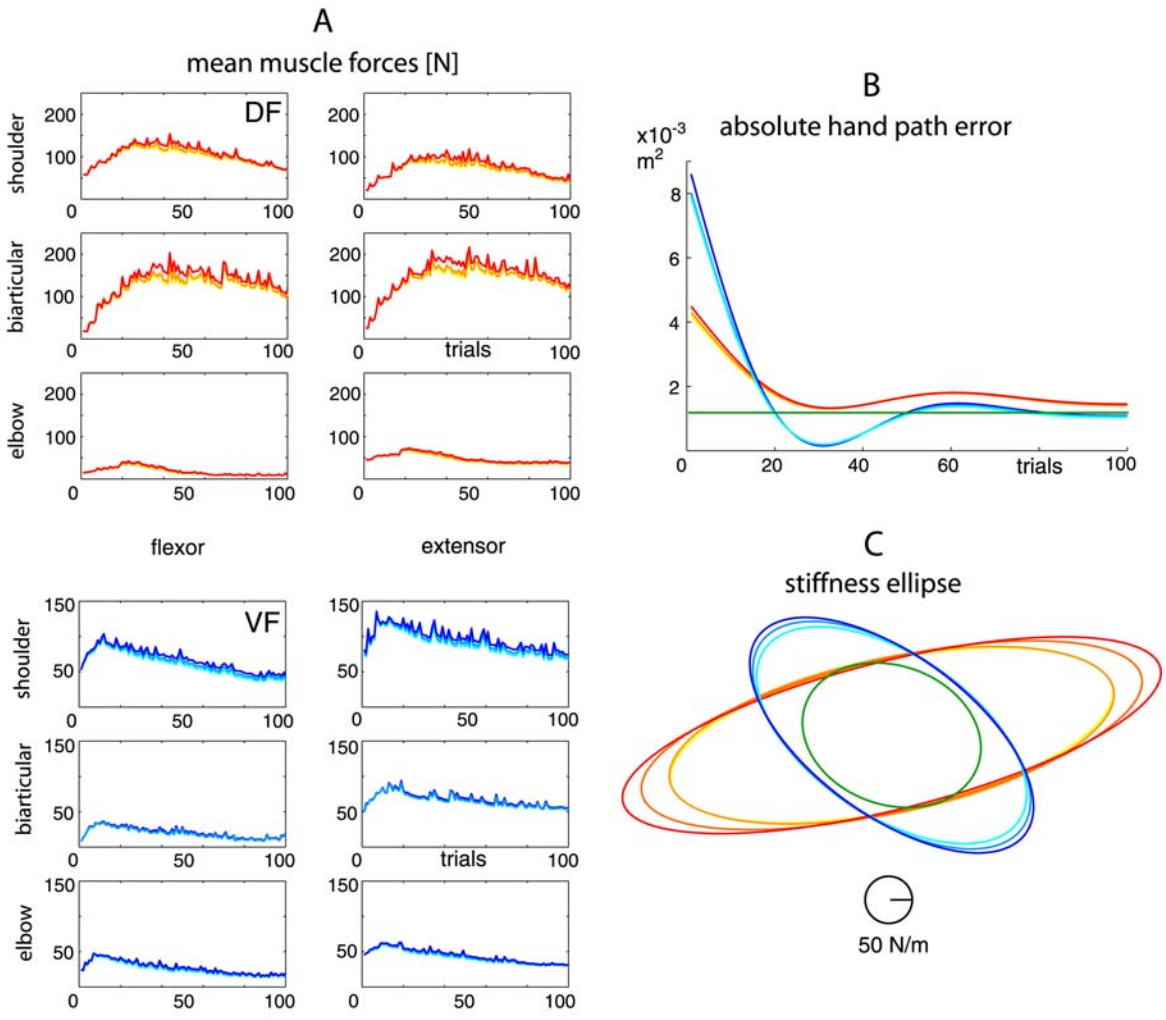

Fig. 15 Sensitivity to reflex delay. For VF, delays of 60, 100, and 200ms are represented by light blue, medium blue and dark blue respectively. For DF, delays of 60, 100, 150 and 200ms are represented by yellow, light orange, medium orange and red respectively. NF is represented by green. *A*: Evolution of mean muscle forces during adaptation. *B*: Evolution of absolute hand path error during adaptation. *C*: Stiffness after adaptation to novel dynamics.

Fig. 16 illustrates how impedance depends on motor noise. When the noise in (31) is uniformly scaled by a factor s>1, the NF stiffness ellipse is enlarged isomorphically to produce stable movements. When s<1, NF stiffness decreases due to deactivation. Subsequent adaptation in DF produces elongated stiffness increase in the direction of instability. The algorithm learns to increase impedance to guarantee similar deviation in all noise conditions.

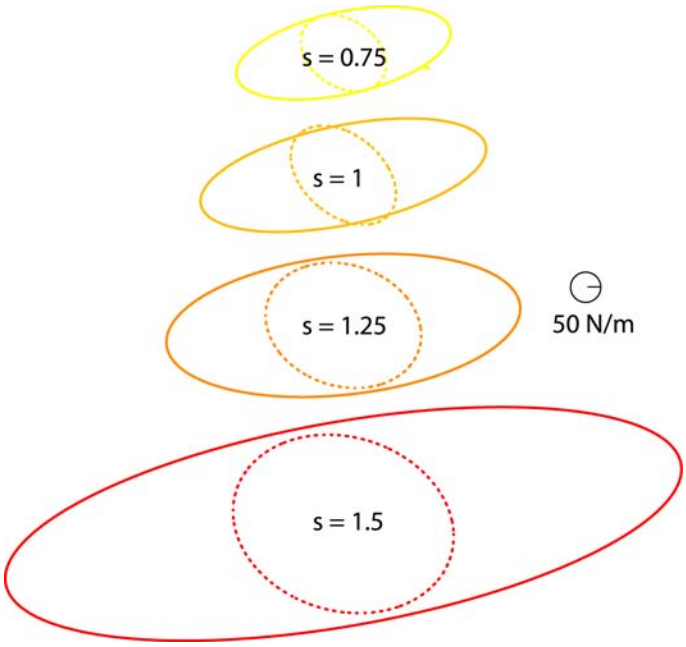

Fig. 16 Coupling between impedance and motor noise. *Dotted*: NF stiffness. *Solid*: stiffness after adaptation to DF. *s* is a scaling factor multiplying noise in (31).

4.2.2 Sensitivity to learning parameters

Cross reflex strength

Fig. 17 shows the sensitivity to the cross reflex strength β. Higher β results in larger cocontraction, as seen in the simultaneous increase of flexor and extensor muscle forces.

The large impedance obtained after adaptation reduces movement deviation. Also, high β results in low reflex torque and hence a slow decrease of kinematic error in interactions requiring modification of torque. This explains the slow adaptation to VF and the large build-up of muscle force. When β is zero, i.e. there is no cross reflex, adaptation to DF is still successful, yielding sufficient stiffness to compensate for instability.

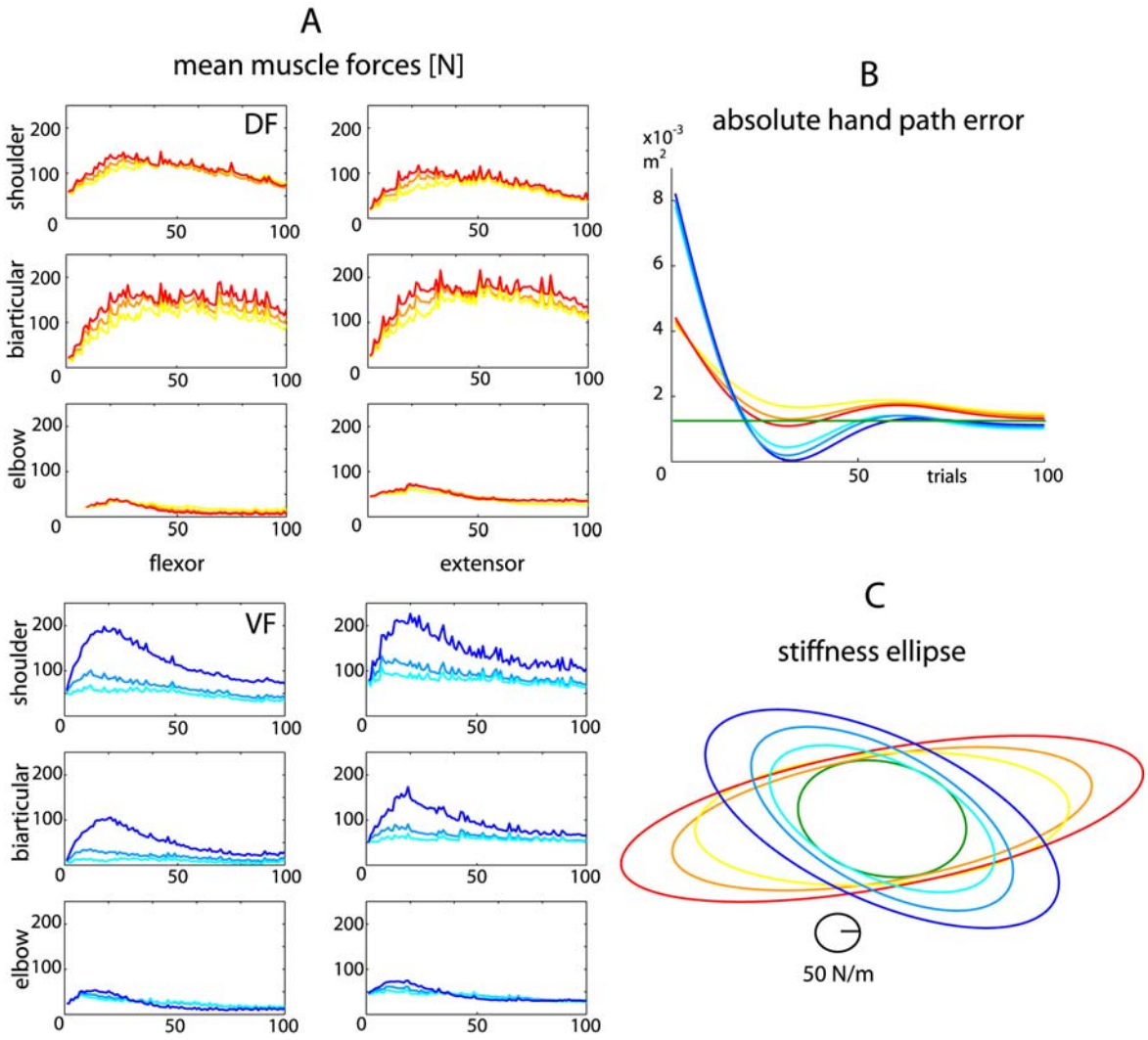

Fig. 17 Sensitivity to cross reflex strength β. The β values of 0, 0.4 and 0.8 are represented by light, medium and dark blue respectively for VF and by yellow, orange and red respectively for DF. NF is represented by green. *A*: Evolution of mean muscle forces during adaptation. *B*: Evolution of absolute hand path error during adaptation. *C*: Stiffness after adaptation to novel dynamics.

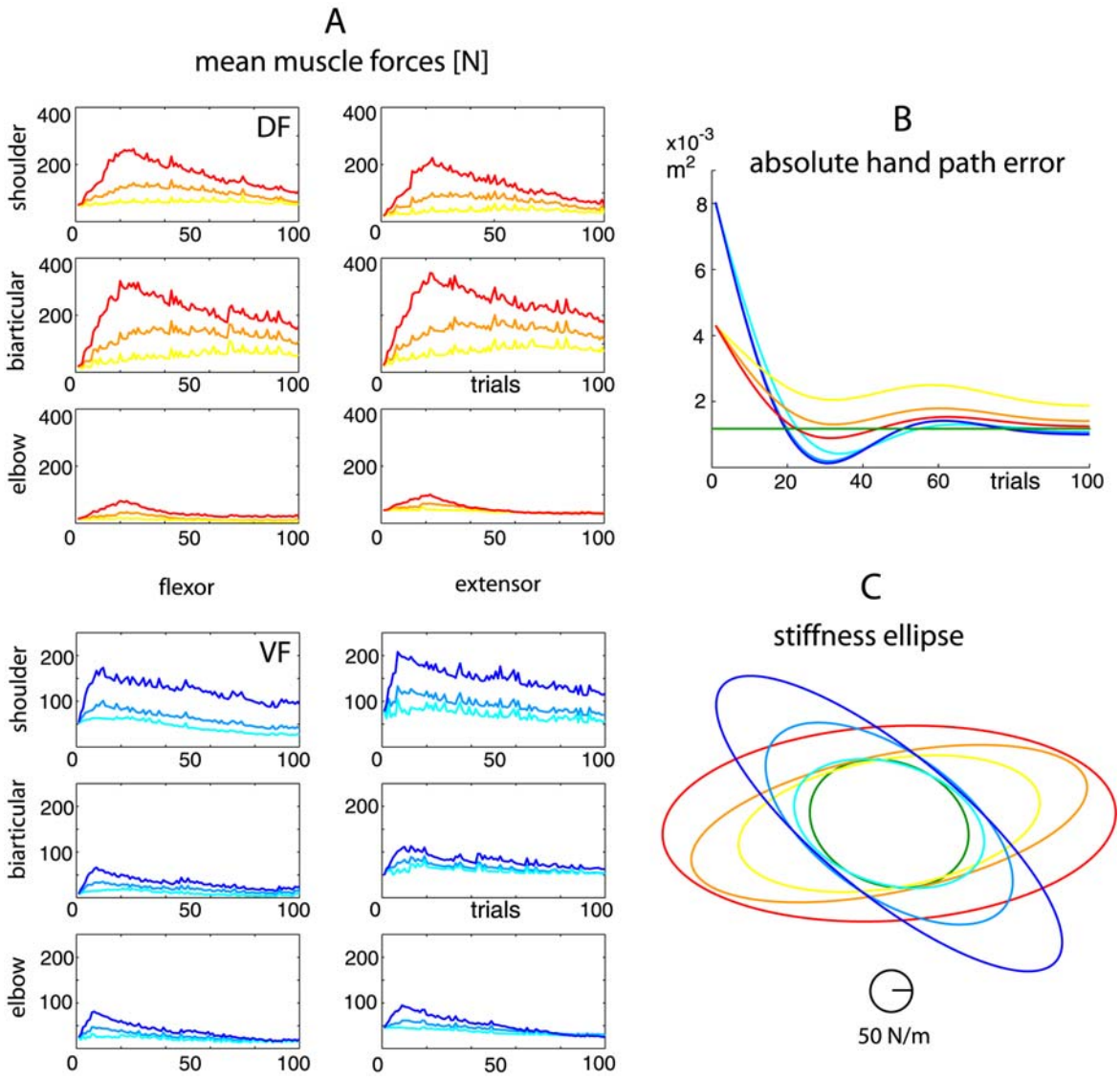

Fig. 18 Sensitivity to learning factor α_0. The α_0 values of 1, 3 and 6 are represented by light, medium and dark blue respectively for VF and by yellow, orange and red respectively for DF. NF is represented by green. *A*: Evolution of mean muscle forces during adaptation. *B*: Evolution of absolute hand path error during adaptation. *C*: Stiffness after adaptation to novel dynamics.

Learning factor and decay rate

Fig. 18 shows the sensitivity to the learning factor α_0. When α_0 increases, there is an overall increase of muscle forces and a decrease of absolute hand path error. This trend can be seen in both the transient and final adaptation. A higher α_0 gives faster rise time, larger maximum overshoot and higher steady state value. The final stiffness increases as

α_0 increases. When α_0 is too low, learning in DF is unsuccessful since the final stiffness is not sufficiently large to compensate for the instability. This can be seen in the absolute hand path error, which is significantly higher than that of NF.

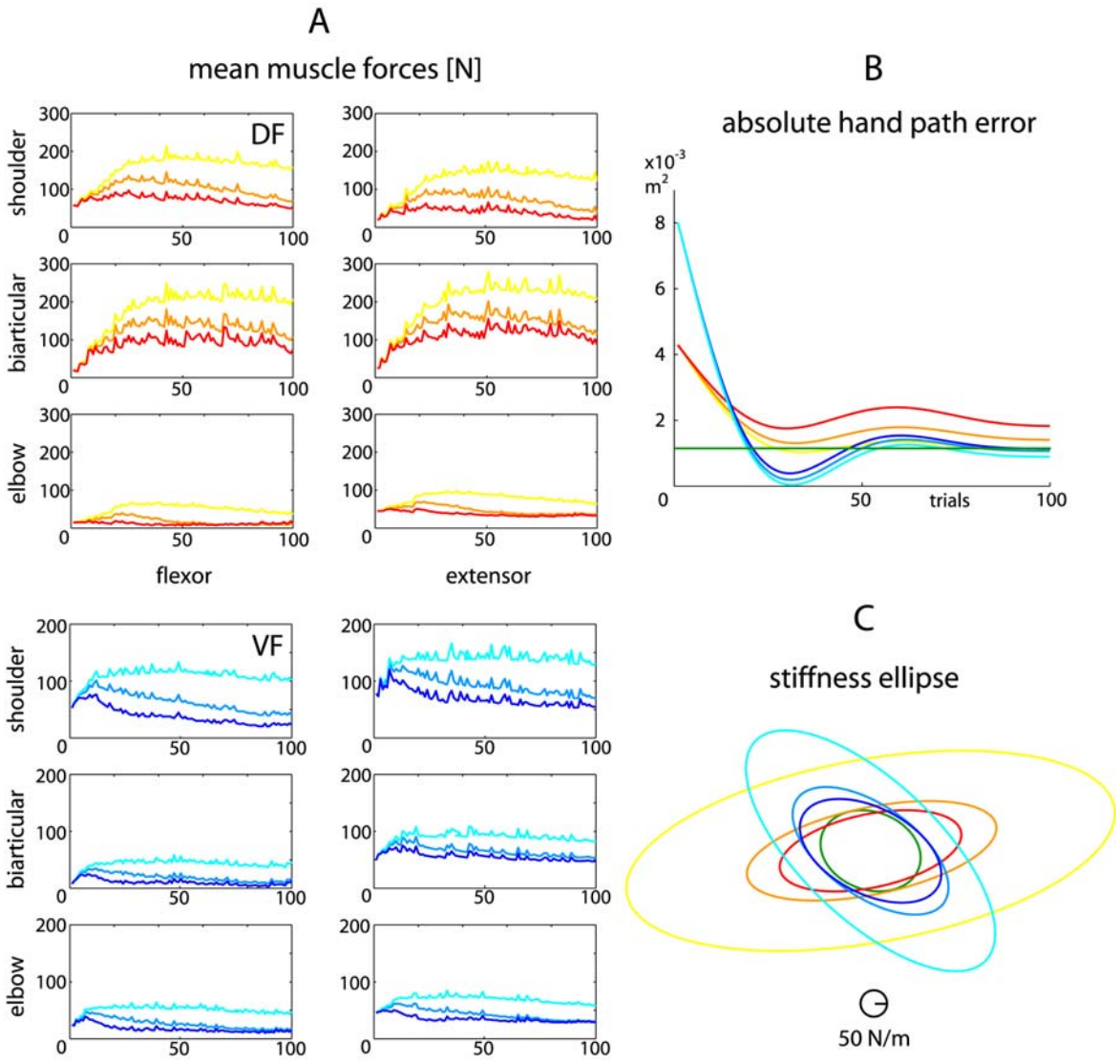

Fig. 19 Sensitivity to decay rate γ_0. The γ_0 values of 0.01, 0.04 and 0.08 are represented by light, medium and dark blue respectively for VF and by yellow, orange and red respectively for DF. NF is represented by green. *A*: Evolution of mean muscle forces during adaptation. *B*: Evolution of absolute hand path error during adaptation. *C*: Stiffness after adaptation to novel dynamics.

Fig. 19 shows the sensitivity to the decay rate γ_0. It can be seen that a low γ_0 results in a slow rate of decrease of muscle forces. The final stiffness is large and the hand path error is small. Conversely, high γ_0 prevents sufficient increase of stiffness to compensate for the instability in DF, resulting in movements that are unsuccessful even after extensive learning.

While α_0 and γ_0 have different effects on the transients of learning, their effects on the final stiffness are similar. Large asymptotic stiffness results from either a large α_0 or a small γ_0, and small asymptotic stiffness results from the converse relationship. Therefore the size of the adapted stiffness increases with the ratio α_0/γ_0. A large ratio leads to excessive stiffness increase that is more than required to stabilise motion. A small ratio results in inadequate increase of stiffness in DF and unsuccessful movements even after a long learning phase.

Relative decay ratio

Fig. 20 shows the sensitivity to the relative decay ratio γ_1. γ_1=1 corresponds to independent deactivation in all muscle pairs, described in (23), and results in shoulder and elbow muscle activity being larger than required. This yields stiffness that is not reduced even in relatively stable directions. γ_1=0.33 corresponds to homogenous deactivation described in (24) and results in large muscle forces in the biarticular muscles for DF and in the shoulder muscles for VF. These muscle pairs have large activities because they are maximally stretched in the respective force fields. The activities in other muscle pairs decrease rapidly. γ_1=0.7 gives a more moderate build-up of activity in the muscle pair that is maximally stretched. At the same time, the activities in the other muscle pairs do not

decrease so rapidly. As γ_1 decreases, the adapted stiffness becomes increasingly elongated along the stiffness axis of the maximally stretched muscle pair. There is faster decay of activity in all muscle pairs except the pair that is primarily stretched, which experiences an increasing build-up.

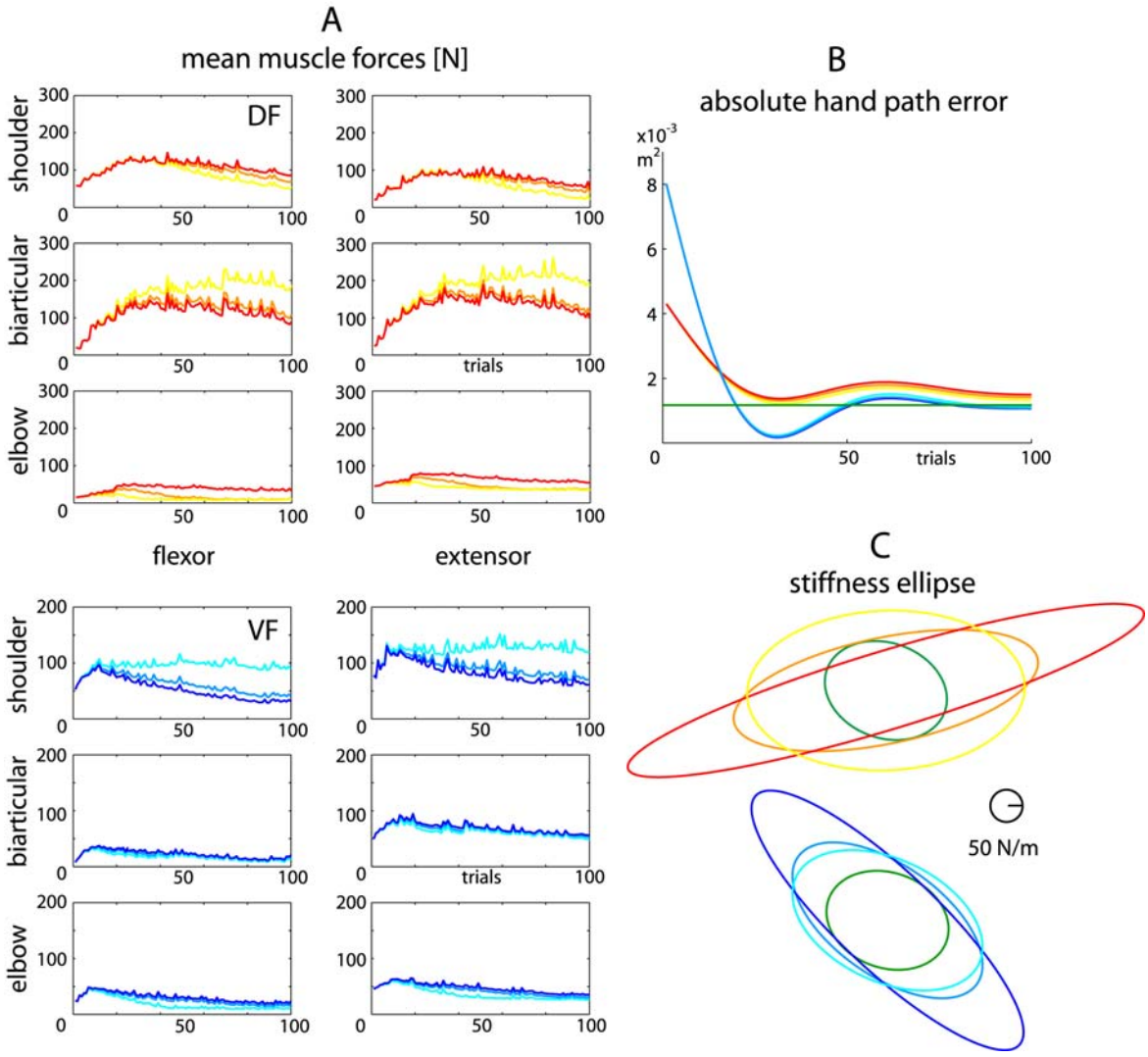

Fig. 20 Sensitivity to relative decay factor γ_1. The γ_1 values of 0.33, 0.7 and 1are represented by light, medium and dark blue respectively for VF and by yellow, orange and red respectively for DF. NF is represented by green. *A*: Evolution of mean muscle forces during adaptation. *B*: Evolution of absolute hand path error during adaptation. *C*: Stiffness after adaptation to novel dynamics.

4.2.3 Robustness of model

In summary, the novel algorithm is robust to large variations of the parameters. Reflex and muscle elasticity parameters, which ensure good control performance in NF produce good learning in stable and unstable dynamics. In particular, the algorithm is able to learn to perform stable motion in unstable dynamics. To our knowledge this is the first algorithm with such adaptation property.

Despite a large increase of noise and reflex delay, which have potentially destabilising effects, neither learning nor motion control are impeded. The algorithm is able to deal with an increase in noise of up to 150% and a reflex delay of up to 200ms (well above the physiological range), by increasing impedance to produce stable movements with deviation similar to NF motion.

The transients and asymptotic impedance depend on the learning parameters. Adaptation is successful with various values of cross reflex strength β from 0 to 1, and various ratios of learning to deactivation α_0/γ_0 from 50 to 120, producing qualitative evolution features that are generally similar to experimental results (Burdet *et al* 2001A, Franklin *et al* 2003A, Osu *et al* 2003, Franklin *et al* 2003B).

4.3 Model Predictions

This section shows the results that are predicted by the model in novel dynamics (other than VF and DF) for which only partial or no experimental data are available. The predicted results may be tested in future experiments. Two questions are addressed in this section:

i. Our impedance adaptation algorithm relies on the strategy that gives an increase of endpoint stiffness in approximately the same direction as the deviation (Section 2.7). At the same time, the winner-takes-all deactivation strategy tends to minimize cocontraction in the muscles that are minimally stretched. In view of the two complementary strategies, does the model generally predict a stiffness increase in the direction of instability?

ii. The novel dynamics used so far are either purely stable (VF) or purely unstable (DF). We have seen that inverse dynamics are learnt to compensate for stable dynamics whereas impedance is increased to counteract instability (Section 4.1). Is the model able to concurrently learn the inverse dynamics and impedance so as to adapt to composite interactions comprising both stable and unstable dynamics? What does it learn in this case?

4.3.1 Unstable interactions with different directions of instability

To address the first question, three force fields are examined: $DF_{\{\theta=135°\}}$, $DF_{\{\theta=80°\}}$, $DF_{\{\theta=45°\}}$. They are similar to DF except that the destabilizing forces act along the axis θ degrees relative to the x-axis. The axis along which the hand experiences zero external force is unchanged i.e. {x=0}. The mean external force is approximately zero as the hand diverges left and right of {x=0} and thus adaptation is due to the increase of impedance brought about by cocontraction of agonist and antagonist muscles. The strengths of the various DF fields are chosen such that the corresponding trajectory deviations are adequately unstable. The directions of instability {θ=135°}, {θ=80°} and {θ=45°} are chosen such that the task space is spanned. With instability along {θ=90°}, movements

are seriously impeded since they are along the same direction. Hence {θ=80°} is chosen instead. These directions allow us to test if the algorithm consistently produces an increase of stiffness in the direction of instability.

DF$_{\{\theta=135°\}}$

The external force is given by

$$\begin{bmatrix} F_x \\ F_y \end{bmatrix} = -350 \begin{bmatrix} x \\ -x \end{bmatrix} \tag{36}$$

The initial movements diverge unpredictably left and right of the centerline but tend to travel farther in the positive y-direction on the left side (Fig. 21). Movements after adaptation successfully reach the target and are similar to NF movements.

Reciprocal activation levels are roughly constant in all muscles, and the after effects are similar to NF movements, showing that successful adaptation is not due to learning an inverse dynamics model of the external force. Rather, it is due to the increase of arm impedance produced by cocontraction of agonist and antagonist muscles. Cocontraction level in the shoulder muscle pair increased maximally, while those for the biarticular and elbow pairs are relatively lower. This is because the imposed stretch experienced in the shoulder muscles, from (19), is substantially larger than in the other two pairs.

To test if the direction of stiffness increase is aligned with the direction of instability {θ=135°}, we compare the adapted stiffness with the theoretical stiffness obtained by

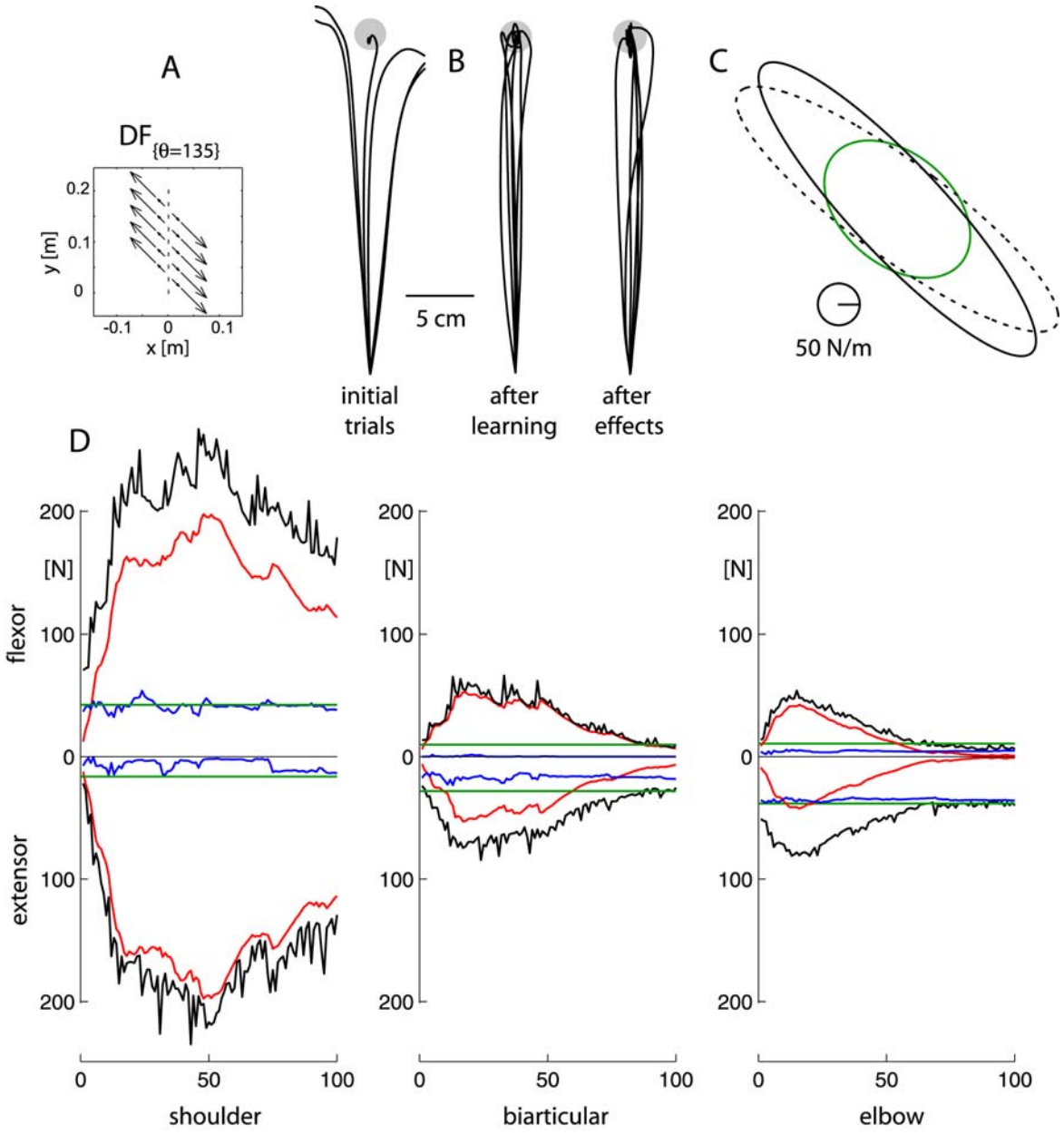

Fig. 21 Simulated adaptation to $DF_{\{\theta=135°\}}$. *A*: Vector field of external force as a function of hand position. *B*: Hand trajectories in initial and final adaptation, as well as after effects of adaptation. *C*: Adapted endpoint stiffness (black, solid) and NF stiffness (green). The dotted ellipse is the stiffness obtained by increasing the NF stiffness in the direction of the instability. *D*: Evolution of mean muscle forces (black) over 100 learning trials in DF. Green lines represent the mean muscle force levels in NF movements. Blue and red represent mean levels of reciprocal activation and cocontraction respectively.

increasing the NF stiffness in the direction of the instability (Fig. 21C). The magnitude of increase is such that the maximum eigenvalues of the theoretical and adapted stiffness are

the same. It can be seen that the orientations of the adapted and theoretical stiffness are similar, showing that stiffness increases approximately in the direction of the instability. With our algorithm, the maximal stretch of shoulder muscles induces maximal build-up of cocontraction in the shoulder muscles, providing an increase of stiffness in the shoulder pair stiffness axis (see Fig. 10), to counteract the instability in approximately the same direction.

$DF_{\{\theta=80°\}}$

The external force is given by

$$\begin{bmatrix} F_x \\ F_y \end{bmatrix} = -175 \begin{bmatrix} x \\ x \tan 80° \end{bmatrix} \tag{37}$$

The initial trajectories diverge and tend to overshoot the target when the hand is in the right half but fall short of the target when in the left half (Fig. 22). The large perturbation in the y-direction causes a large disparity in the y-displacement between the left and right halves of the workspace. The adaptation of movements is successful, giving trajectories that are similar to NF movements.

Reciprocal activation levels are roughly constant in all muscles, and the after effects are similar to NF movements, showing that successful adaptation is not due to learning an inverse dynamics model of the external force. Rather, it is due to the increase of arm impedance produced by cocontraction of agonist and antagonist muscles. Cocontraction levels in the elbow and biarticular pairs are large after adaptation because they are substantially stretched in this direction of destabilization. In contrast, shoulder muscle forces decreased to a low level since they are minimally stretched.

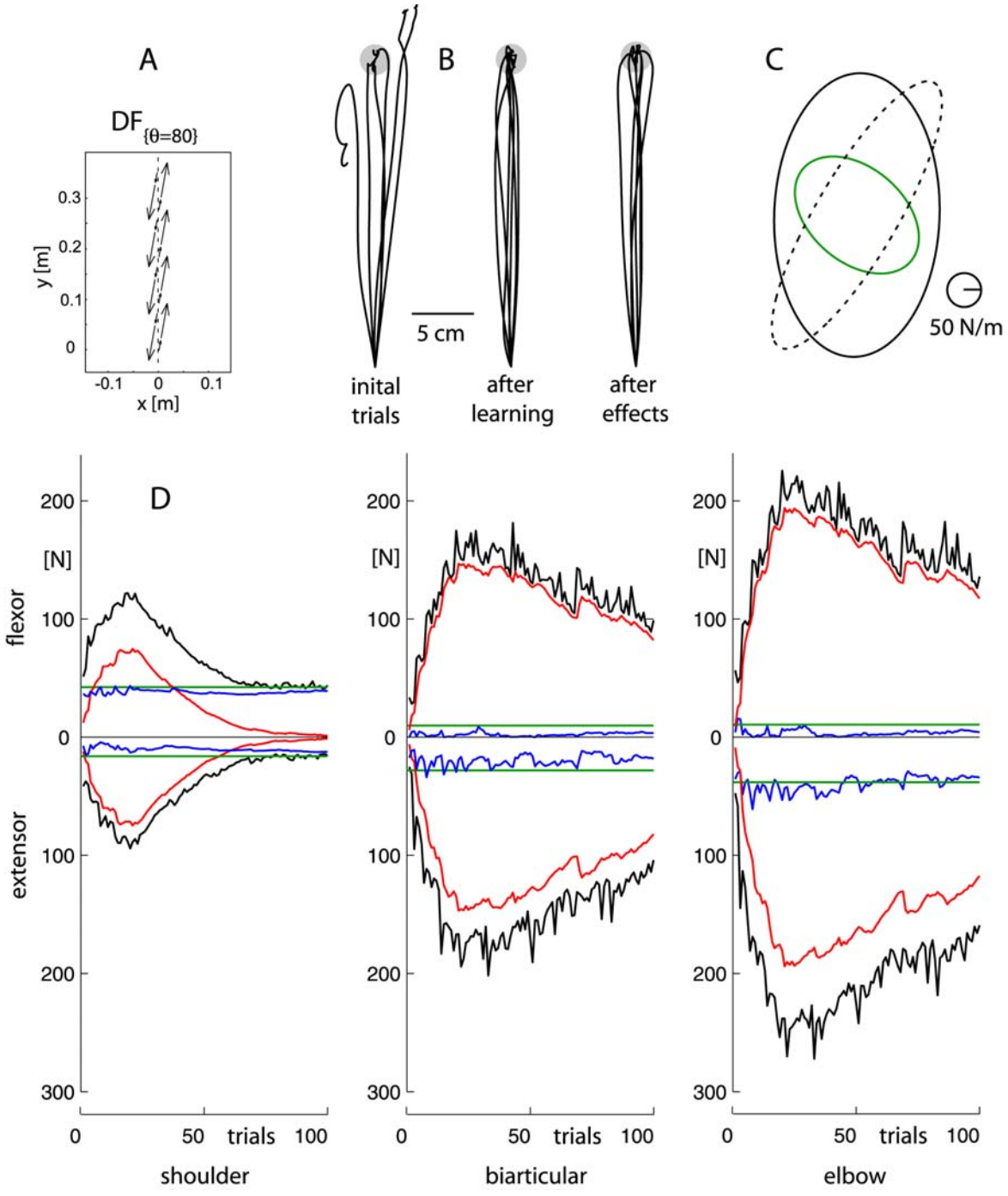

Fig. 22 Simulated adaptation to $DF_{\{\theta=80°\}}$. *A*: Vector field of external force as a function of hand position. *B*: Hand trajectories in initial and final adaptation, as well as after effects of adaptation. *C*: Adapted endpoint stiffness (black, solid) and NF stiffness (green). The dotted ellipse is the stiffness obtained by increasing the NF stiffness in the direction of the instability. *D*: Evolution of mean muscle forces (black) over 100 learning trials in DF. Green lines represent the mean muscle force levels in NF movements. Blue and red represent mean levels of reciprocal activation and cocontraction respectively.

In comparison with the theoretical stiffness obtained by increasing the NF stiffness in the direction of the instability, the adapted stiffness has approximately the same orientation (Fig. 22C). With our algorithm, the maximal stretch of elbow muscles induces maximal build-up of cocontraction in the elbow pair, producing an increase of stiffness primarily in the direction of the elbow stiffness axis, which is similar to the direction of instability {θ=80°}. However, there is also a moderate increase of stiffness along {θ=0°} because the substantial stretch of the biarticular muscle pair elicits a moderately high cocontraction level. As a result, the adapted stiffness does not 'touch' the NF ellipse and appears to be non-minimal.

$DF_{\{\theta=45°\}}$

The external force is given by

$$\begin{bmatrix} F_x \\ F_y \end{bmatrix} = -280 \begin{bmatrix} x \\ x \end{bmatrix} \tag{38}$$

As shown in Fig. 23, the initial movements diverge unpredictably left and right of the centerline but tend to travel farther in the positive y-direction on the right side. This is expected since the external force perturbs the hand in the positive y-direction when in the right half and in the negative y-direction when in the left half. Adapted movements are similar to NF movements.

Reciprocal activation levels are roughly constant in all muscles, and the after effects are similar to NF movements, showing that successful adaptation is not due to learning an inverse dynamics model of the external force. Rather, it is due to the increase of arm impedance produced by cocontraction of agonist and antagonist muscles. Cocontraction

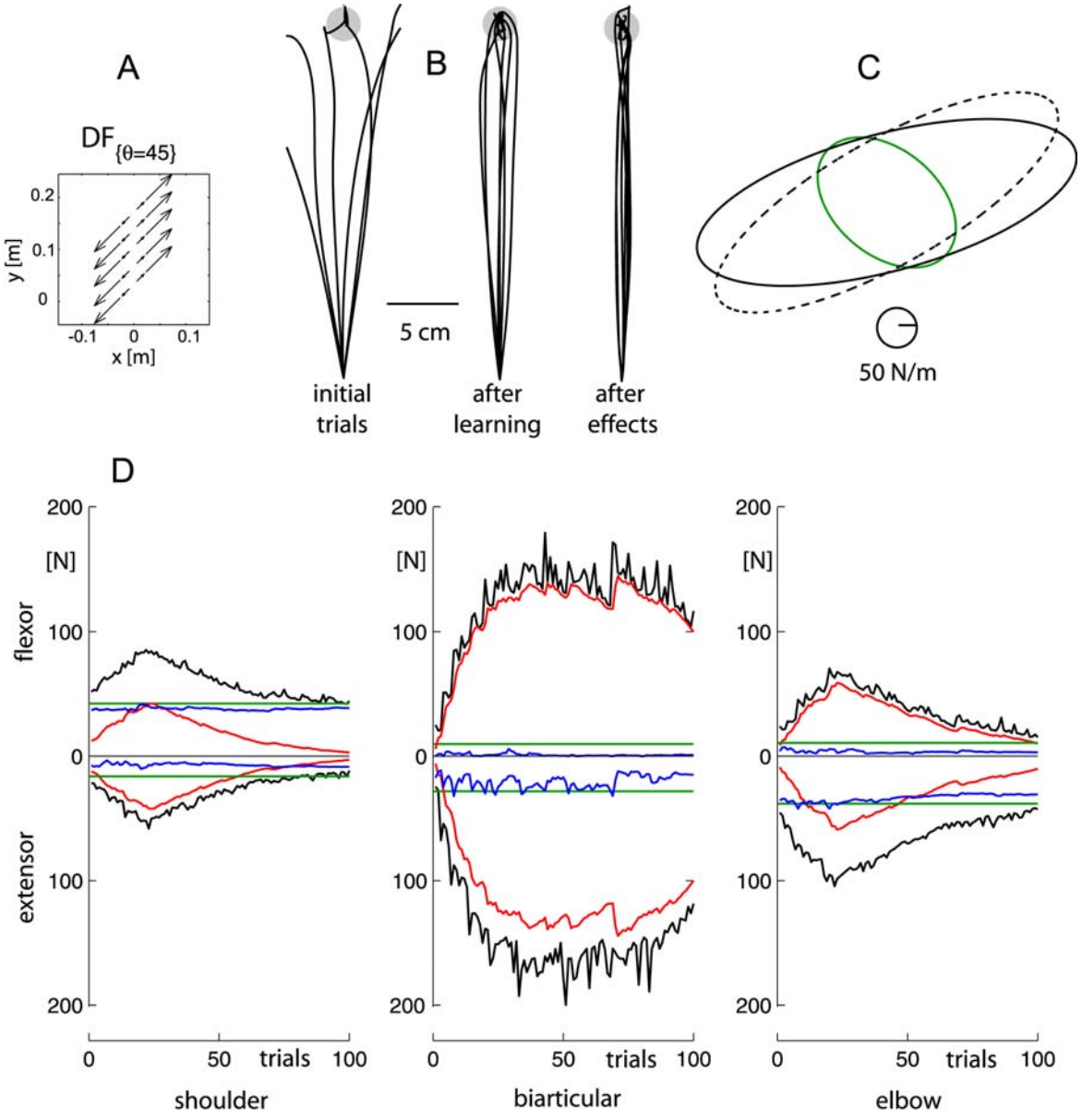

Fig. 23 Simulated adaptation to $DF_{\{\theta=45°\}}$. *A*: Vector field of external force as a function of hand position. *B*: Hand trajectories in initial and final adaptation, as well as after effects of adaptation. *C*: Adapted endpoint stiffness (black, solid) and NF stiffness (green). The dotted ellipse is the stiffness obtained by increasing the NF stiffness in the direction of the instability. *D*: Evolution of mean muscle forces (black) over 100 learning trials in DF. Green lines represent the mean muscle force levels in NF movements. Blue and red represent mean levels of reciprocal activation and cocontraction respectively. Note that in this case the adapted stiffness is not oriented at 45°.

level in the biarticular pair is large after adaptation because the biarticular muscles are maximally stretched when the instability is along {θ=45°}, as can be verified from (19). In

contrast, the cocontraction forces in the shoulder and elbow muscle pairs decreased to low levels since the muscles are stretched by a relatively less amount.

The adapted stiffness has approximately the same orientation as the theoretical stiffness obtained by increasing the NF stiffness in the direction of the instability (Fig. 23C). With our algorithm, the maximal stretch of biarticular muscles induces maximal build-up of cocontraction in the biarticular pair, producing an increase of stiffness primarily in the direction of the biarticular stiffness axis, leading to successful adaptation to instability along $\{\theta=45°\}$.

From the simulated adaptation to the three force fields $DF_{\{\theta=135°\}}$, $DF_{\{\theta=80°\}}$, and $DF_{\{\theta=45°\}}$, it can be deduced that impedance generally increases in the direction of instability. However, this does not mean that impedance is optimized in Cartesian space. In fact, our winner-takes-all algorithm performs optimization in muscle space, minimizing cocontraction levels in all but those muscle pairs that are maximally stretched. The large build-up of cocontraction in each maximally stretched muscle pair provides an increase of stiffness along its stiffness axis (Fig. 10). Hence there is a tendency for the orientation of the adapted stiffness to align with the stiffness axis of the muscle pair being stretched maximally, as seen in the simulated results. Because the muscle pair stiffness axes are generally well distributed in the task space, given our set of moment arms, any direction of instability will be near to one of the stiffness axes. This accounts for the fact that impedance generally increases in the direction of instability.

4.3.2 Composite interactions comprising stable and unstable dynamics

To address the second question of whether the algorithm is able to adapt to composite interactions consisting of both stable and unstable dynamics, two force fields are examined: rDF and rCF. Each has the same direction of destabilization as DF but the axis along which there is no external force (i.e. zero-force axis) is rotated. The rDF is a divergent field with zero-force axis rotated 7° and the rCF is a convergent field with zero-force axis rotated -7°. Both rotations are relative to the y-axis. With rotated zero-force axis, the arm would have to compensate for a bias force as well as instability.

rDF

The external force is given by

$$\begin{bmatrix} F_x \\ F_y \end{bmatrix} = -350(x\cos 7^\circ + (y-0.31)\sin 7^\circ)\begin{bmatrix} \cos 7^\circ \\ \sin 7^\circ \end{bmatrix} \tag{39}$$

Due to the leftward bias force, the initial trajectories are perturbed towards the left, as shown in Fig. 24. After adaptation, the trajectories are straight. After effect trajectories deviate towards the right, showing that an inverse dynamics model has been acquired in the learning. This is consistent with the experimental results of (Osu *et al* 2003).

Simulated muscle activity is similar to that in DF except for the large increase of reciprocal activation in the biarticular extensor muscle to compensate for the leftward bias force. The shoulder extensor muscle has a relatively smaller increase of reciprocal activation. Similar to DF adaptation, the stiffness is elongated approximately along {θ=0°}, with a stiffness margin relative to NF that is large in the x-direction and

negligible in the y-direction. The deviation of after effects motion relative to the centerline is reduced as a result of this increase of impedance.

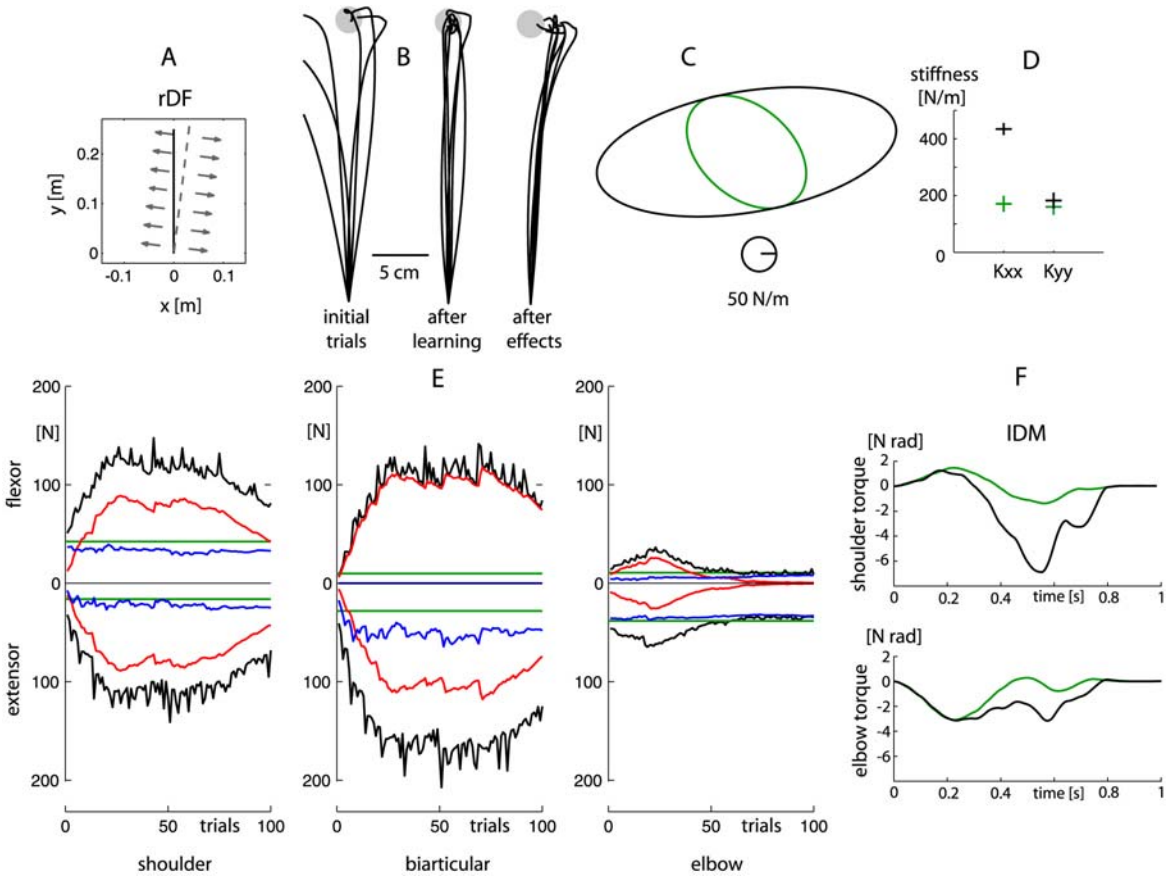

Fig. 24 Simulated adaptation to rDF. *A*: Vector field of external force as a function of hand position. *B*: Hand trajectories in initial and final adaptation, as well as after effects of adaptation. *C*: Adapted endpoint stiffness (black) and NF stiffness (green). *D*: The K_{xx} and K_{yy} stiffness components after adaptation are shown in black whereas those for NF are shown in green. *E*: Evolution of mean muscle forces (black) over 100 learning trials in DF. Green lines represent the mean muscle force levels in NF movements. Blue and red represent mean levels of reciprocal activation and cocontraction respectively.

rCF

The external force is given by

$$\begin{bmatrix} F_x \\ F_y \end{bmatrix} = 350(x\cos(-7^\circ) + (y - 0.31)\sin(-7^\circ))\begin{bmatrix} \cos(-7^\circ) \\ \sin(-7^\circ) \end{bmatrix} \quad (40)$$

Initial trajectories are perturbed to the left due to the leftward bias force that is the same as in the rDF (Fig. 25). After adaptation in about 10 trials, the trajectories are fair straight. After effects trajectories deviate towards the right, corresponding to experimental results of (Osu *et al* 2003), and showing that an inverse dynamics model has been acquired.

Mean muscle forces in the flexors decreased below the initial levels after adaptation due to a decrease in both the reciprocal activation and the cocontraction components. For the extensors, there is an increase in the mean levels of reciprocal activation, mostly in the biarticular muscles. As a result of similar bias force, the increase of reciprocal activation levels and the mean after effects trajectories in both rCF and rDF are similar.

The converging field provides an increase of stability to the system that reduces the trajectory deviation due to noise. This leads to a decrease of cocontraction in all muscle pairs below their initial levels, giving a slightly reduced stiffness. As a result, the deviation of after effects motion relative to the centerline is increased.

It can be seen that the reduction of stiffness in the x-direction is almost negligible while the reduction in the y-direction is relatively larger. In view of the fact that rCF and rDF have the same strength, how is it that the magnitude of stability margin (the net difference between the adapted and NF stiffness) of rCF is much smaller than that of rDF?

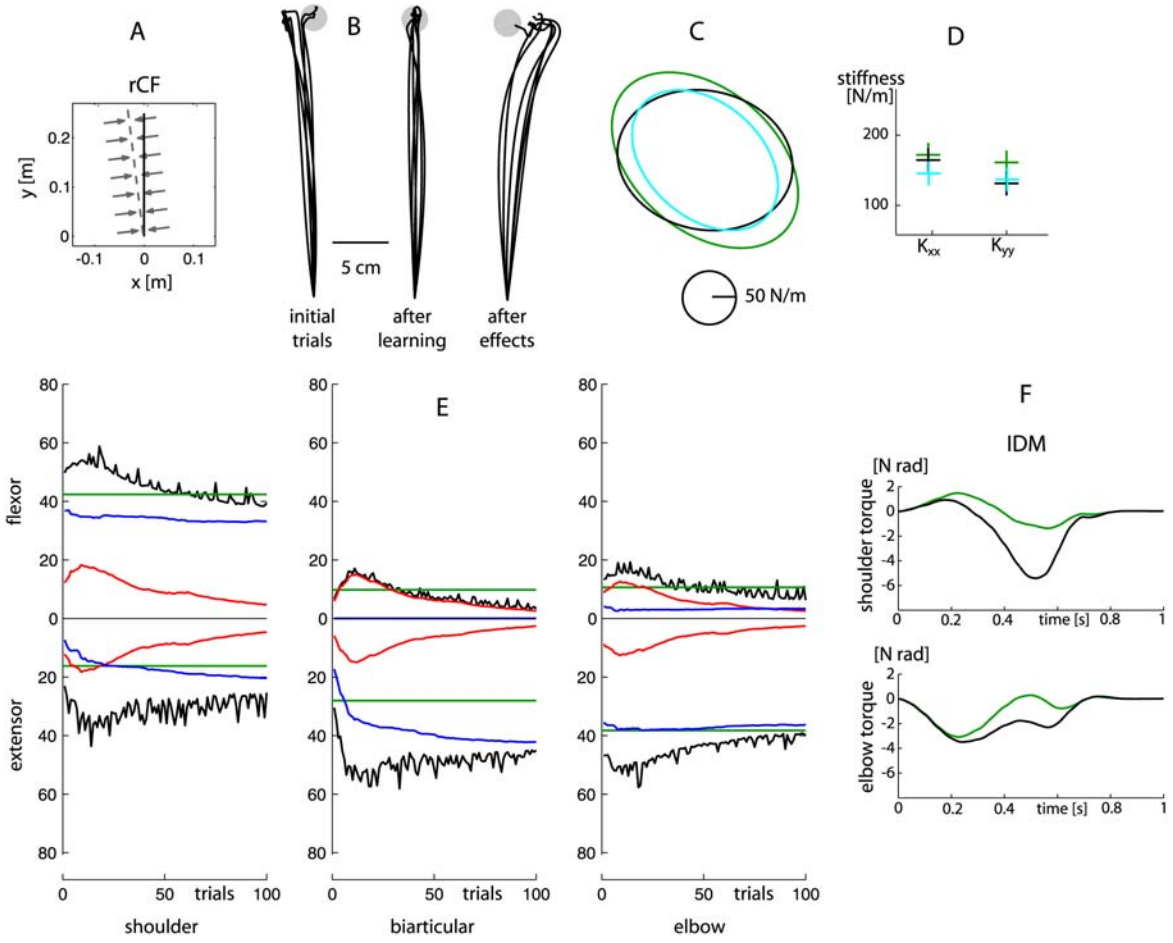

Fig. 25 Simulated adaptation to rCF. *A*: Vector field of external force as a function of hand position. *B*: Hand trajectories in initial and final adaptation, as well as after effects of adaptation. *C*: Adapted endpoint stiffness (black) and NF stiffness (green). The cyan ellipse is the stiffness after adaptation to CF i.e. convergent field without bias force. *D*: The K_{xx} and K_{yy} stiffness components after adaptation to rCF and CF are shown in black and cyan respectively whereas the same stiffness components for NF are shown in green. *E*: Evolution of mean muscle forces (black) over 100 learning trials in DF. Green lines represent the mean muscle force levels in NF movements. Blue and red represent mean levels of reciprocal activation and cocontraction respectively.

Stiffness reduction in rCF is limited as there is a minimal stiffness arising from passive muscle tissue, from movement dynamics, and from compensation of the bias force. The latter two arise due to the obligatory coupling between force and stiffness (Hunter and Kearney 1982, Gomi and Osu 1998). To test if the negligible change of K_{xx} is due to the compensation of the bias force, we simulated adaptation to a pure convergent field CF, defined by $\mathbf{F}_{CF} = (350x, 0)$, that does not comprise any bias force. Indeed, we see

a significant decrease of the K_{xx} component when the external bias force is removed. This shows that the negligible change of K_{xx} in rCF is attributed to bias force compensation.

The adaptations to rCF and rDF clearly show that the algorithm is able to concurrently learn the inverse dynamics of reproducible external forces as well as the necessary impedance against irreproducible external forces.

5 Discussion

This thesis has introduced a novel model of motor adaptation using the stretch reflex to modulate the feedforward muscle activation and selective deactivation to decrease superfluous agonist-antagonist co-activation. The simulations show that this model is successful in adapting to various stable and unstable novel dynamics, and produces changes in motion, impedance, and muscle activity highly consistent with experimental results. While conventional feedback error learning only learns the inverse dynamics and so cannot compensate for unstable dynamics, the novel algorithm, extending feedback error learning, simultaneously learns the endpoint force and impedance necessary to perform stable motions, as illustrated in the adaptation to force fields producing both a bias force and instability (Figs. 24 and 25).

5.1 Stiffness magnitude depends on noise amplitude and environmental instability

The controller adapts to the current environment and learns to produce trajectories with similar deviation in all environments, which is consistent with the experimental results (Burdet *et al* 2001A, Osu *et al* 2003, Franklin *et al* 2003C). An interesting prediction of the model is that impedance increases with motor noise (Fig. 16), and similarly with environment instability (Fig. 14). This is because the algorithm is only concerned with deviation and not the source of this deviation. An interesting experiment would be to increase motor noise (for example by vibrating muscles) and ascertain if impedance would, in reality, increase as predicted by our model.

5.2 Role of cross reflexes

Experimental results (Franklin *et al* 2003A, Osu *et al* 2003, Franklin *et al* 2003B) have shown evidence for cross reflexes, i.e. there is an increase of antagonist muscle activity even though only the agonist muscle is stretched. Obviously cross reflexes produces cocontraction, and thus stabilization. To test whether cross reflex is necessary to ensure successful adaptation to unstable dynamics, we decreased the cross reflex strength β down to zero for the adaptation to DF. The results show that even without impedance provided by cross reflexes, adaptation to unstable dynamics is still successful, and is realized at a lower level of muscle activity (Fig. 17). In fact, most of the impedance required for stabilizing motion stems from the coupling of feedback error learning with instability, through the build-up of activity in agonist and antagonist muscles over a series of consecutive alternating movements. From a control perspective, it can be argued that the utility of cross reflexes reflects the importance of stability in the strategy employed by the CNS when adapting to novel dynamics, such that it justifies a higher metabolic cost. Perhaps such provision of a larger-than-required stability margin is required to facilitate the formation of an inverse dynamic model (Franklin *et al* 2003B).

5.3 Selective deactivation strategy

A given deviation of the hand imposes a stretch on various muscles in the arm. Through feedback error learning at the muscle level, the stretched muscles increase activity, resulting in an increase of endpoint impedance generally in the direction of deviation. However, the increase of impedance in the other directions is larger than what is observed

in (Burdet *et al* 2001A). Hence, a selective deactivation strategy is required such that superfluous impedance not required for task stabilization is reduced.

The winner-takes-all deactivation strategy used in our model minimizes cocontraction in the muscle pairs that are minimally stretched. Only the muscle pairs that are substantially stretched will retain the cocontraction muscle activity required for task stabilization. In this way, it provides for anisotropic increase of impedance that is large in the direction of instability and small in the other directions. This is observed in the simulated adaptation to DF and to other divergent fields with different directions of instability.

While we do not know what the CNS is optimizing exactly, experimental results support the idea that the CNS is able to control the impedance size, shape and orientation through appropriate muscle co-activation. In our algorithm, for simplicity, we have fixed the cocontraction pairings such that $\Delta m_{c1}=\Delta m_{c2}$, $\Delta m_{c3}=\Delta m_{c4}$, and $\Delta m_{c5}=\Delta m_{c6}$ at all times, with Δm_c denoting the change of cocontraction muscle activity. The effect of cocontraction of each fixed pair on endpoint stiffness, shown in Fig. 10, restricts the possible impedance geometry. For example, consider a desired stiffness change along 45° from the x-axis, which is in between the biarticular and elbow pair stiffness axes. Cocontraction of either the biarticular or the elbow muscles increases stiffness only along the respective muscle pair stiffness axis. Cocontraction of both the biarticular and elbow pairs results in a generalized increase of stiffness in more than one direction. Therefore, with fixed muscle pairings, it is not possible to achieve a stiffness change exactly along 45°, and likewise for any direction other than those corresponding to the three muscle pair

stiffness axes. It is interesting to note that despite such constraints arising from our simplification, preliminary experimental results are consistent with these findings.

We could give more freedom for coactivation without modifying endpoint force, for example producing changes in muscle activity satisfying the following equations:

$$\Delta\tau_1=\rho_1\Delta m_{c1} - \rho_2\Delta m_{c2} + \rho_5\Delta m_{c5} - \rho_6\Delta m_{c6}=0$$

$$\Delta\tau_2=\rho_3\Delta m_{c3} - \rho_4\Delta m_{c4} + \rho_7\Delta m_{c5} - \rho_8\Delta m_{c6}=0$$

This would allow a greater set of possible muscle pair stiffness axes that will satisfy optimal stiffness control. Despite the theoretical possibilities, it remains unclear whether the CNS is able to activate muscles independently to achieve coordinated, synergistic control of impedance.

5.4 Ideal and realistic deactivation

Another limitation of the model is that in the deactivation strategy, only cocontraction is decreased and not the reciprocal activation. In a post-adaptation behavioral study (Scheidt *et al* 2000), it was shown that the adapted muscle activity, corresponding to the inverse dynamics of the stable interaction, undergoes slow relaxation when the movements are constrained within a straight channel. The relaxation is much slower than in normal conditions without the channel, i.e. when kinematic error is provided. In the absence of kinematic error, our algorithm can only rely on deactivation to produce the change in motor command. With a decrease of only cocontraction and not the reciprocal activation in each agonist-antagonist muscle pair, no change of endpoint force will occur with our model. We suggest that in reality the CNS is not able to perform such perfectly

coordinated deactivation without a change of endpoint force. The associated change of endpoint force with the decrease of cocontraction may suffice to produce the gradual unlearning of the inverse dynamics model as observed in (Scheidt *et al*. 2000), even without kinematic error.

5.5 Conclusion

Despite the limitations, the novel algorithm of motor adaptation is robust to large variations of the parameters. While transients and asymptotic impedance depend on the learning parameters, the qualitative evolution features are generally similar to the experimental results (Burdet *et al* 2001A, Franklin *et al* 2003A, Osu *et al* 2003, Franklin *et al* 2003B). The simulations show a large increase of coactivation in initial trials, followed by a gradual decrease, and a selective increase of impedance in the direction of instability. Furthermore, the physiologically-based parameter values result in learning and control patterns that are quantitatively consistent with what have been measured. Such computational models, using measurable variables, may be used as tools to investigate the neural control of posture and movement, to simulate the effect of neuro-muscular disorders on control, to develop better controllers for neural prostheses, and to develop robot-assisted rehabilitation protocols.

References

Albus, J.S. (1975)
A New Approach to Manipulator Control: The Cerebellar Model Articulation Controller. Journal of Dynamical Systems, Measurements, and Control 97, 220-227.

Bayard D. and Wen J.T. (1998)
A New Class of Stabilizing Control Laws for Robotic Manipulators, Part II: Adaptive Case. International Journal of Control, 47(5), pp.1387-1406

Bien, Z. and Xu, J.X. (1998)
Iterative Learning Control. Academic Publishers.

Burdet E., Tee K.P., Chew C.M., Mareels I., Milner T.E., Osu R., Franklin D. and Kawato M. (2003)
Stability and learning in human movements. Internal report. Department of Mechanical Engineering. National University of Singapore.

Burdet E., Osu R., Franklin D.W., Milner T.E. and Kawato M. (2001)A
The CNS skillfully stabilizes unstable dynamics by learning optimal impedance. Nature 414: 446-449.

Burdet E., Tee K.P., Chew C.M., Franklin D.W., Osu R. and Kawato M., Milner T.E. (2001)B
Stability and learning in human arm movements. Proc Int Conf on Computational Intelligence, Robotics and Autonomous Systems 355-360.

Burdet E., Tee K.P., Chew C.M., Franklin D.W., Osu R., Kawato M. and Milner T.E. (2001)C
Hybrid IDM/impedance learning in human movements. Int Symposium on measurement, analysis and modeling of human functions 340-345.

Burdet E., Osu R., Franklin D.W., Yoshioka T., Milner T.E. and Kawato M. (2000)
A method for measuring endpoint stiffness during multi-joint arm movements. J Biomech 33(12): 1705-1709

Burdet E., Codourey A. and Rey L. (1998)
Experimental evaluation of nonlinear adaptive controllers. IEEE Control Systems Magazine. April: 39-69.

Burdet E. (1996)
Algorithms of human motor control and their implementations in robotics. PhD Thesis, ETH Zurich.

Carter R.R., Crago P.E. and Keith M.W. (1990)
Stiffness regulation by reflex action in the normal human hand. J Neurophysiol 64:105-118.

Collins J.J. (1995)
The redundant nature of locomotor optimization laws. J Biomech 28:251-267.

Conditt M.A. and Mussa-Ivaldi F.A. (1997)
The motor system does not learn the dynamics of the arm by rote memorization of past experience. J Neurophysiol. 78(1):554-60.

de Serres S.J. and Milner T.E. (1991)
Wrist muscle activation patterns and stiffness associated with stable and unstable mechanical loads. Exp Brain Res 86:451-458.

de Waal F.B.M. (1999)
Cultural primatology comes of age, Nature 399, 635 - 636 (17 Jun 1999) News and Views

de Wit C.C., Siciliano B. and Bastin G. (1996)
Theory of robot control. Springer, NY.

Diffrient N., Tillery A.R. and Bardagjy J.C. (1978)
Humanscale. Cambridge MA: MIT press.

Eng J.J. and Hoffer J.A. (1997)
Regional variability of stetch reflex amplitude in the cat medial gastrocnemius muscle during a postural task. J Neurophysiol 78:1150-1154.

Franklin D.W., Burdet E., Osu R., Kawato M. and Milner T.E. (2003)A
Functional significance of stiffness in adaptation of multijoint arm movements to stable and unstable dynamics. Exp Brain Res 151:145-157.

Franklin D.W., Osu R., Burdet E., Kawato M. and Milner T.E. (2003)B
Adaptation to stable and unstable dynamics achieved by combined impedance control and inverse dynamics model. J Neurophysiol 90: 3270 - 3282.

Franklin D.W., So U., Kawato M. and Milner T.E. (2003)C
Interacting with our environment: impedance control balances stability and metabolic cost. Proc 25th IEEE Engineering in Medicine and Biology Ann Int Conf (in press).

Franklin D.W., Burdet E., Tee K.P., Osu R., Kawato M. and Milner T.E. (2002)
A computational model of adaptation to novel stable and unstable dynamics. Ann Conf of the Neuroscience Society.

Franklin D.W. (2002)
System identification and stability analysis of the interaction between the human limb and PFM in velocity-dependent force fields. Internal report. Computational Neuroscience Project. Advanced Telecommunications Research Institute International.

Festinger M.L. and Canon L.K. (1965)
Information about spatial location based on knowledge about efference. Psychol Rev 72: 373-384.

Fitts P.M. (1954)
The information capacity of the human motor system in controlling the amplitude of movements. J. Exp Psychol 47:381-391.

Foley J.M. and Held R. (1972)
Visually directed pointing as a function of target distance, direction and available cues. Percept Psychohys 12: 263-268.

Gomi H. and Osu R. (1998)
Task-dependent viscoelasticity of human multijoint arm and its spatial characteristics for interaction with environments. J Neurosc 18: 8965-9878.

Gomi H., Shidara M., Tekemura A., Inoue Y., Kitama H., Kawano K. and Kawato M. (1998)
Temporal firing patterns of Purkinje cells in the cerebellar ventral parafloccus during ocular following responses in monkeys. I. Simple spike. J. Neurophysiol 80: 818-831.

Gomi H. and Kawato M. (1997)
Human arm stiffness and equilibrium point trajectory during multi-joint movement. Biol Cyb 76(3): 163-71

Hunter I.W. and Kearney R.E. (1982)
Dynamics of human ankle stiffness: variation with displacement amplitude. J. Biomech 15:753-756.

Lee R.G. and Tatton W.G. (1982)
Long latency reflexes to imposed displacements of the human wrist: dependence on duration of movement. Exp Brain Res 45:207-216

Jones K.E., Hamilton A. and Wolpert D.M. (2001)
Sources of signal-dependent noise during isometric force production. J Neurophysiol 88: 1533-1544.

Kawato M., Furukawa K. and Suzuki R. (1987)
A hierarchical neural-network model for control and learning of voluntary movement. Biol Cybern 57: 169-185.

Kawato M. (1999)
Internal models for motor control and trajectory planning. Curr Opin Neurobiol 9: 718-727.

Kobayashi Y., Kawano K., Takemura A., Inoue Y., Kitama T., Gomi H. and Kawato M. (1998)
Temporal firing patterns of Purkinje cells in the cerebellar ventral parafloccus during ocular following responses in monkeys. II. Ventral spikes. J. Neurophysiol 80: 832-848.

Krakauer J.W., Ghilardi M.F. and Ghez C. (1999)
Independent learning of internal models for kinematic and dynamic control of reaching. Nat Neurosci 2:1026–1031

Pedotti A. (1978)
Optimization of muscle-force sequencing in human locomotion. Mathematical Bioscience 38:57-76.

Marsaglia G. and Tsang W.W. (1984)
A fast, easily implemented method for sampling from decreasing or symmetric unimodal density functions. SIAM Journal of Scientific and Statistical Programming, Volume 5, No. 2.

Meyer D.E., Abrams R.A., Kornblum S., Wright C.E. and Smith J.E.K. (1998)
Optimality in human motor performance: ideal control of rapid aimed movements. Psychol Rev 98: 340-370.

Milner T.E. and Cloutier C. (1993)
Compensation for mechanically unstable loading in voluntary wrist movement, Exp Brain Res 94: 522-532.

Milner T.E., Cloutier C., Leger A.B. and Franklin D.W. (1995)
Inability to activate muscles maximally during cocontraction and the effect on joint stiffness. Exp Brain Res 107:293-305.

Nakano E., Harris C.M. and Kawato M. (2002)
Task optimization in the presence of signal-dependent noise: impedance control. Internal report. Information Sciences Division. Advanced Telecommunications Research Institute International.

Nakazawa K., Yamamoto S., Ohtsuki, T., Yano H. and Fukunaga, T. (2001)
Neural control: novel evaluation of stretch reflex sensitivity. Acta Physiol Scand 172:257-268.

Osu R., Burdet E., Franklin D.W., Milner T.E. and Kawato M. (2003)
Different mechanisms involved in adaptation to stable and unstable dynamics. J Neurophysiol 90: 3255 - 3269.

Scheidt R.A., Reinkensmeyer, D.J., Conditt M.A., Rymer, W.Z. and Mussa-Ivaldi F.A. (2000)
Persistence of motor adaptation during constrained, multi-joint, arm movements. J. Neurophysiol 84:853-862.

Schmidt R.A., Zelaznik H., Hawkin B., Frank J.S., and Quinn J.T. (1979)
Motor-output variability: a theory for the accuracy of rapid motor acts. Psychol Rev 86: 415-451.

Shadmehr R. and Mussa-Ivaldi F.A. (1994)
Adaptive representation of dynamics during learning of motor tasks. J Neurosci 14(5): 3208-3224.

Shadmehr R. and Holcomb H.H. 1997)
Neural correlates of motor memory consolidation. Science 277(5327): 821-825.

Shidara M., Kawano K., Gomi H. and Kawato M. (1993)
Inverse-dynamics encoding of eye-movements of Purkinje cells in the cerebellum. Nature365: 50-52.

Sinkjaer T., Toft E., Andreassen S. and Hornemann B.C. (1988)
Muscle stiffness in human ankle dorsiflexors: intrinsic and reflex components. J. Neurophysiol 60:1110-1121.

Stroeve, S. (1999)
Impedance Characteristics of a Neuromuscoloskeletal Model of the Human Arm II. Movement Control. Biol Cybern, 81:495-504.

Tee K.P. (2001)
A hybrid IDM/impedance learning controller to stabilise unstable dynamics. B.A. Eng Thesis. Department of Mechanical Engineering. National University of Singapore.

Tee K.P., Burdet E., Chew C.M. and Milner T.E. (2003A)
Investigating Motor Adaptation to Stable and Unstable Tasks Using Haptic Interfaces, EMG and fMRI. The Society of Instrument and Control Engineers Ann Conf.

Tee K.P., Burdet E., Chew C.M. and Milner T.E. (2003B)
A model of endpoint force and impedance in human arm movements. Internal report. Department of Mechanical Engineering. National University of Singapore.

van Beers R.J., Sittig A.C. and Denier van der Gon J.J. (1998)
The precision of proprioceptive position sense. Exp Brain Res 122: 367-377.

van Beers R.J., Baraduc P. and Wolpert D.M. (2002)
Role of uncertainty in sensorimotor control. Phil Trans Royal Soc Lond B 357: 1137-1145.

Weir, A.A.S., Chappell, J. and Kacelnik, A. (2002)
Shaping of hooks in New Caledonian crows. Science, 297: 981.

Whiten A., Goodall J., McGrew W. C., Nishida T., Reynolds V., Sugiyama Y., Tutin C. E. G., Wrangham R. W. and Boesch C. (1998)
Cultures in chimpanzees. Nature 399: 682–685.

Wolpert D.M., Ghahramani Z. and Jordan M.I. (1995)
An internal model for sensorimotor integration. Science 269: 1880-1882.

Yamamoto K., Kobayashi Y., Takemura A. and Kawano K. (2001)
Compuational studies on acquisition and adaptation of ocular following responses based on cerebellar synaptic plasticity. J. Neurophysiol 87: 1554-1571.

Appendix A: Kinematic Transformations

In hand space, $\mathbf{x}\equiv(x,y)$ is the hand position, and $\mathbf{F}\equiv(F_x,F_y)$ the force exerted on the hand. In joint space, $\mathbf{q}\equiv(q_s,q_e)$ is the joint position, $\mathbf{q}_v\equiv(q_{v,s},q_{v,e})$ the joint velocity, and $\boldsymbol{\tau}\equiv(\tau_s,\tau_e)$ the joint torque. Subscripts $_s$ and $_e$ denote the shoulder and elbow joints respectively. In muscle space, $\boldsymbol{\lambda}\equiv(\lambda_1,\lambda_2,\lambda_3,\lambda_4,\lambda_5,\lambda_6)$ is the vector of muscles lengths, $\boldsymbol{\lambda}_v\equiv(\lambda_{v,1},\lambda_{v,2},\lambda_{v,3},\lambda_{v,4},\lambda_{v,5},\lambda_{v,6})$ the corresponding velocity and $\mathbf{m}\equiv(m_1,m_2,m_3,m_4,m_5,m_6)$ the muscle tensions.

1. The inverse kinematics equations ($\mathbf{x}\rightarrow\mathbf{q}$) of the 2-joint, 2-segment arm used in our simulations are:

$$q_e = \cos^{-1}\left(\frac{x^2+y^2-l_1^{\,2}-l_2^{\,2}}{2l_1l_2}\right), \qquad \text{for } 0<q_e<\pi \tag{A1}$$

$$\psi = \cos^{-1}\left(\frac{x^2+y^2+l_1^{\,2}-l_2^{\,2}}{2l_1\sqrt{x^2+y^2}}\right), \qquad \text{for } 0<\psi<\pi/2$$

$$q_s = \mathrm{a}\tan 2\left(\frac{y}{x}\right)-\psi \tag{A2}$$

2. The Jacobian transformation relating an infinitesimal change in hand position to an infinitesimal change in joint position($d\mathbf{q}\rightarrow d\mathbf{x}$) is expressed as:

$$\mathbf{J}=\left(\frac{\partial \mathrm{x_i}}{\partial \mathrm{q_j}}\right)=\begin{bmatrix} -l_1\sin q_s - l_2\sin(q_s+q_e) & l_2\sin(q_s+q_e) \\ l_1\cos q_s + l_2\cos(q_s+q_e) & l_2\cos(q_s+q_e)\end{bmatrix}$$

3. The transformation between joint torque and endpoint force ($\mathbf{F}\rightarrow\boldsymbol{\tau}$) is derived, using the principle of conservation of energy, as follows

$\boldsymbol{\tau}^T \delta\mathbf{q} = \mathbf{F}^T \delta\mathbf{x}$

$\boldsymbol{\tau} = (\mathbf{F}^T(\delta\mathbf{x}/\delta\mathbf{q}))^T$

$\boldsymbol{\tau} = \mathbf{J}^T\mathbf{F}$

4. The transformation between joint stiffness and endpoint stiffness ($\mathbf{K}_x \rightarrow \mathbf{K}_q$) is derived as:

$$\mathbf{K}_q = \frac{d\boldsymbol{\tau}}{d\mathbf{q}} = \frac{d(\mathbf{J}^T\mathbf{F})}{d\mathbf{q}}$$

$$= \mathbf{J}^T \frac{\partial \mathbf{F}_i}{\partial \mathbf{x}_j} \frac{\partial \mathbf{x}_j}{\partial \mathbf{q}_k} + \frac{d\mathbf{J}^T}{d\mathbf{q}}\mathbf{F}$$

$$= \mathbf{J}^T \mathbf{K}_x \mathbf{J} + \frac{d\mathbf{J}^T}{d\mathbf{q}}\mathbf{F}$$

5. The change in muscle lengths is related to the change in joint position ($\delta\mathbf{q} \rightarrow \delta\boldsymbol{\lambda}$) by:

$$\begin{bmatrix} \delta\lambda_1 \\ \delta\lambda_2 \\ \delta\lambda_3 \\ \delta\lambda_4 \\ \delta\lambda_5 \\ \delta\lambda_6 \end{bmatrix} = \begin{bmatrix} \rho_1 \delta q_s \\ -\rho_2 \delta q_s \\ \rho_3 \delta q_e \\ -\rho_4 \delta q_e \\ \rho_5 \delta q_s + \rho_7 \delta q_e \\ -\rho_6 \delta q_s - \rho_8 \delta q_e \end{bmatrix}$$

or $\delta\boldsymbol{\lambda} = \mathbf{J}_m \delta\mathbf{q}$, with $\mathbf{J}_m = \left(\frac{\partial \lambda_i}{\partial q_j}\right) = \begin{bmatrix} \rho_1 & -\rho_2 & 0 & 0 & \rho_5 & -\rho_6 \\ 0 & 0 & \rho_3 & -\rho_4 & \rho_7 & -\rho_8 \end{bmatrix}^T$

6. The transformation between joint torque and muscle tension ($\mathbf{m} \rightarrow \boldsymbol{\tau}$) is

$$\begin{bmatrix} \tau_s \\ \tau_e \end{bmatrix} = \begin{bmatrix} \rho_1 m_1 - \rho_2 m_2 + \rho_5 m_5 - \rho_6 m_6 \\ \rho_3 m_3 - \rho_4 m_4 + \rho_7 m_5 - \rho_8 m_6 \end{bmatrix}$$

or $\boldsymbol{\tau} = \mathbf{J}_m{}^T \mathbf{m}$

7. The transformation between joint stiffness and muscle stiffness ($\mathbf{K}_m \rightarrow \mathbf{K}_q$) is derived as:

$$\mathbf{K}_q = \frac{d\boldsymbol{\tau}}{d\mathbf{q}} = \frac{d(\mathbf{J}_m{}^T \mathbf{m})}{d\mathbf{q}}$$

$$= \mathbf{J}_m{}^T \frac{\partial \mathbf{m}_i}{\partial \boldsymbol{\lambda}_j} \frac{\partial \boldsymbol{\lambda}_j}{\partial \mathbf{q}_k}$$

$$= \mathbf{J}_m{}^T \mathbf{K}_m \mathbf{J}_m$$

Appendix B: Rigid Body Dynamics Model

This Appendix describes the rigid body dynamics of a 2-joint, 2-segment arm moving on the horizontal plane. Let M denote the segment mass, J denote the segment inertia, l its length, l_{m} the distance between the center of mass of the segment and the proximal joint, with subscripts $_1$ and $_2$ denoting the upper arm and forearm respectively, and subscripts $_{\mathrm{s}}$ and $_{\mathrm{e}}$ denote the shoulder and elbow joints respectively. The rigid body dynamics is expressed in the following form:

$$\boldsymbol{\tau}(\mathbf{q}, \dot{\mathbf{q}}, \ddot{\mathbf{q}}) = \mathbf{H}(\mathbf{q})\ddot{\mathbf{q}} + \mathbf{C}(\mathbf{q}, \dot{\mathbf{q}})\dot{\mathbf{q}}$$

where the inertia matrix $\mathbf{H}(\mathbf{q})$ is represented as:

$$\mathbf{H}(\mathbf{q}) = \begin{bmatrix} J_1 + J_2 + M_1 l_{\mathrm{m1}}{}^2 + M_2(l_1{}^2 + l_{\mathrm{m2}}{}^2 + 2l_1 l_{\mathrm{m2}} \cos q_{\mathrm{e}}) & J_2 + M_2(l_{\mathrm{m2}}{}^2 + l_1 l_{\mathrm{m2}} \cos q_{\mathrm{e}}) \\ J_2 + M_2(l_{\mathrm{m2}}{}^2 + l_1 l_{\mathrm{m2}} \cos q_{\mathrm{e}}) & J_2 + M_2 l_{\mathrm{m2}}{}^2 \end{bmatrix}$$

and the term $\mathbf{C}(\mathbf{q}, \dot{\mathbf{q}})\dot{\mathbf{q}}$, corresponding to Corioli's and centrifugal forces, is represented as:

$$\mathbf{C}(\mathbf{q}, \dot{\mathbf{q}})\dot{\mathbf{q}} = \begin{bmatrix} -M_2 l_1 l_{\mathrm{m2}} \dot{q}_e (2\dot{q}_{\mathrm{s}} + \dot{q}_{\mathrm{e}}) \sin q_{\mathrm{e}} \\ M_2 l_1 l_{\mathrm{m2}} \dot{q}_{\mathrm{s}}{}^2 \sin q_{\mathrm{e}} \end{bmatrix}$$

Appendix C: Summary of Equations and Parameter Values

Dynamic Equations

The *dynamics of the arm* moving while interacting with the environment is described by

BODY + FORCE = SPRING + FF + NOISE + REFLEX, (A1)

corresponding to the scheme of Fig. 3. Muscles have to produce the rigid-BODY dynamics to move the limb and to counteract the external FORCE. SPRING corresponds to mechanical impedance (the resistance to infinitesimal perturbation of the state) produced by muscles mechanics. The motor command consists of a feedforward (FF) term that is learned to produce the expected task dynamics, inherent motor NOISE and REFLEXES.

The *elastic force* in every muscle is modeled as a proportional-and-derivative term of the stretch $\lambda(t)$: for each muscle

$$\text{spring}(t) = \kappa\,[\Delta\lambda(t) + \kappa_d\,\Delta\lambda_v(t)]\; I_{\{\Delta\lambda(t)>0\}} \qquad \text{(A2)}$$

where κ is the muscle stiffness, κ_d is the ratio of muscle viscosity to stiffness, I is the Kronecker indicator function defined by $I_{\text{condition}} \equiv 1$ when the *condition* is fulfilled and 0 otherwise. The stretch $\Delta\lambda = \lambda - \lambda_d$ is computed relative to the planned trajectory in muscle coordinates, $\{\lambda_d(t)\}$.

The *reflex* r_a and r_{aa} in the agonist and antagonist muscles of a muscle pair acting at the same joint are modeled as

$$r_a(t) = e_a(t) + \beta\, e_{aa}(t) \qquad \text{(A3)}$$

$r_{aa}(t) = e_{aa}(t) + \beta\, e_a(t)$, where

$$e_a(t) = g\,[\Delta\lambda(t-\phi) + g_d\,\Delta\lambda_v(t-\phi)]\; I_{\{\Delta\lambda(t)>0\}} \qquad \text{(A4)}$$

$$e_{aa}(t) = g\,[\Delta\lambda(t-\phi) + g_d\,\Delta\lambda_v(t-\phi)]\; I_{\{\Delta\lambda(t)>0\}}$$

are the error signals of the agonist and antagonist muscles (linearly dependent on stretch and stretch velocity), β yields the strength of cross reflexes and ϕ is the reflex delay. The subscripts $_a$ and $_{aa}$ denote agonist and antagonist muscles respectively. Both the intrinsic stiffness κ and the reflex gain g increase linearly with muscle activity. For each muscle,

$$\kappa(t) = \kappa_0 + \kappa_1\, m(t) \qquad \text{and} \qquad g(t) = g_0 + g_1 m(t)\,. \qquad \text{(A5)}$$

where κ_0, κ_1, g_0 and g_1 are chosen to be identical across all muscles.

We model the overall effect of the many different sources of *noise* as deviation in muscle tension. This noise is monotonously increasing with the total motor command m, i.e. the addition of feedforward and reflex:

$$\text{noise}(t) = [\mu_0 + \mu_1 m(t)]\;\mu(t) \qquad \text{(A6)}$$

where $\mu(t)$ is a 125*Hz* low-pass filtered Brownian motion.

The major aspect of our algorithm is to describe *how the feedforward (FF) is learned to compensate the task and environment dynamics*. For each muscle, the reflex r, representative of the novel dynamics, is used to update the feedforward muscle tension m according to

$$m^{k+1}(t) \equiv m^k(t) - \gamma(t) + \alpha\, r(t+\phi) \qquad \text{(A7)}$$

The superscript ^{k} denotes the number of elapsed learning trials, α is the learning factor and γ the deactivation. The learning compensates for the reflex delay ϕ by using an equal phase advance. The learning factor

$$\alpha \equiv \tfrac{1}{2}\alpha_0[1+\tanh(\sigma(\bar{e}^{k}-\varepsilon))] \qquad \text{(A8)}$$

is a sigmoid function of the mean stretch error

$$\bar{e}^{k} \equiv (1-\eta)\,\bar{e}^{k-1} + \eta\, e^{k} \qquad \text{(A9)}$$

$$\text{with } e^{k} \equiv \max_j\{(1/T)\textstyle\int_0^T \Delta\lambda_{j,a}{}^{k}(t) + \Delta\lambda_{j,aa}{}^{k}(t)\,dt\}, \qquad \text{(A10)}$$

T is the movement time. $\Delta\lambda_{j,a}$ and $\Delta\lambda_{j,aa}$ denote the stretch at the agonist and antagonist muscles of pair j. The threshold ε in (A8) prevents the algorithm from learning infinite impedance and reducing motion variability to 0. Deactivation decreases superfluous co-activation using

$$\gamma_i(t) = \gamma_0[\gamma_1\, v_i(t) + \tfrac{1}{2}(1-\gamma_1)\, v_{j1}(t) + \tfrac{1}{2}(1-\gamma_1)\, v_{j2}(t)] \qquad \text{(A11)}$$

where $\gamma_0>0$, $1/3<\gamma_1<1$, and

$$v_j = \tfrac{1}{2}(m_a + m_{aa} - |m_a - m_{aa}|)$$

is the coactivation in the j-th muscle pair, with m_a and m_{aa} representing the tension in the agonist and antagonist muscles respectively. Assuming that the deactivation term does not vary in consecutive trials, one finds

$$u^{k+1} \equiv \rho(m_a{}^{k+1} - m_{aa}{}^{k+1}) = \rho\,[m_a{}^{k} - m_{aa}{}^{k} + \alpha(r_a - r_{aa})] = u^{k} + \alpha\rho\,(r_a - r_{aa}) = u^{k} + \alpha\rho\, FB \qquad \text{(A12)}$$

We recognize classical feedback error learning (Kawato *et al* 1987, Burdet *et al* 1998), in which feedback is used to update the feedforward u.

Parameter values

The model's parameters can be distinguished into three distinct groups: parameters of the rigid-body model, parameters influencing the control during the movement, and learning parameters. The default parameters used in the simulation are:

Rigid body model parameters

- moment arms of $0.028m$ for the shoulder muscles, $0.017m$ for the elbow muscles, and $0.044m$ and $0.0338m$ for the biarticular muscles
- anthropometrical parameters for the arm segments are shown in Table 2.

Control parameters

- muscle elasticity (A2 and A5): $\kappa_d \equiv 1/12$, $\kappa_0 = 2844 Nm^{-1}$, $\kappa_1 = 0.035 m^{-1}$
- reflex gains (A5): $g_d \equiv 2$, $g_0 = 114 Nm^{-1}$, $g_1 = 0.035 m^{-1}$
- reflex delay in (A4): $\phi \equiv 100ms$
- strength of the crossed reflexes in (A3): $\beta \equiv 0.4$
- noise (A6): $\mu_0 \equiv 0.0725N$, $\mu_1 \equiv 6.5$

Learning parameters

- learning factor magnitude (A8): $\alpha_0 \equiv 3$
- threshold error for the learning factor α (A8): $\varepsilon \equiv 5.65 \times 10^{-4} m$
- corresponding time scaling: $\sigma \equiv 5500 m^{-1}$
- error averaging factor (A9): $\eta(k) \equiv \begin{cases} 2/5 & \text{for } k \leq 8 \\ 1/8 & k > 8 \end{cases}$
- decay factors (A11): $\gamma_0 \equiv 0.04$, $\gamma_1 \equiv 0.7$